Estimating Earthquake Location and Magnitude from Seismic Intensity Data

by W. H. Bakun and C. M. Wentworth

Abstract Analysis of Modified Mercalli intensity (MMI) observations for a training set of 22 California earthquakes suggests a strategy for bounding the epicentral region and moment magnitude $\mathbf{M}$ from MMI observations only. We define an intensity magnitude $\mathbf{M}_I$ that is calibrated to be equal in the mean to $\mathbf{M}$. $\mathbf{M}_I = \text{mean} (\mathbf{M}_i)$, where $\mathbf{M}_i = (\text{MMI}_i + 3.29 + 0.0206 * \Delta_i)/1.68$ and Δ_i is the epicentral distance (km) of observation MMI_i. The epicentral region is bounded by contours of $\text{rms} [\mathbf{M}_I] = \text{rms} (\mathbf{M}_I - \mathbf{M}_i) - \text{rms}_0 (\mathbf{M}_I - \mathbf{M}_i)$, where rms is the root mean square, $\text{rms}_0 (\mathbf{M}_I - \mathbf{M}_i)$ is the minimum rms over a grid of assumed epicenters, and empirical site corrections and a distance weighting function are used. Empirical contour values for bounding the epicenter location and empirical bounds for $\mathbf{M}$ estimated from $\mathbf{M}_I$ appropriate for different levels of confidence and different quantities of intensity observations are tabulated. The epicentral region bounds and $\mathbf{M}_I$ obtained for an independent test set of western California earthquakes are consistent with the instrumental epicenters and moment magnitudes of these earthquakes. The analysis strategy is particularly appropriate for the evaluation of pre-1900 earthquakes for which the only available data are a sparse set of intensity observations.

Introduction

The cutting edge of seismology for the past several decades has followed the development of new instrumentation to record the ground motions of earthquakes at ever higher dynamic range and broader bandwidth and the widespread availability of powerful computers to analyze the resulting high-fidelity ground-motion data. In this context, intensity is an anacronism for seismologists because the steps in an intensity scale are defined by qualitative descriptions of the effects of earthquakes on man-made structures, people, and the ground surface; the result is that any linear relation of the integer steps in intensity to ground-motion parameters is fortuitous (Howell and Schulz, 1975). Seismologists cannot ignore intensity, however, because reducing the losses in earthquakes is a primary imperative underlying society's support of seismology, and earthquake losses are what intensity scales describe. Also, it is imperative to understand historic earthquakes if earthquake hazards are to be properly assessed, and nearly all that is known of earthquakes that occurred before the introduction of seismological instrumentation is contained in the qualitative descriptions of earthquake effects that intensity scales were introduced to quantify.

Intensity values have long been used to assign magnitudes through empirical relations determined for recent earthquakes having instrumentally determined magnitudes and seismic moments (e.g., Hanks et al., 1975). Typically, the intensity values are used to define isoseismal lines to separate areas where different intensities have been assigned.

For example, the Modified Mercalli intensity (MMI) V isoseismal line bounds $A_{(V)}$, the area where most sites experience MMI V and greater effects; outside $A_{(V)}$, most sites experience MMI IV and less effects. Magnitudes are then estimated from the size (km^2) of the area $A_{(MMI)}$. Toppozada (1975) presented relationships to estimate magnitude for California earthquakes from $A_{(III)}$, $A_{(V)}$, $A_{(VI)}$, and $A_{(VII)}$ that have been used to assign magnitudes to pre-1900 California earthquakes (Toppozada et al., 1981). Magnitudes determined from $A_{(MMI)}$ are robust estimates when the quantity and spatial distribution of intensity observations are sufficient to determine an $A_{(MMI)}$ with precision.

Practical difficulties can arise in determining $A_{(MMI)}$ from the sparse intensity data sets available for pre-1900 earthquakes in California. Often the quantity and spatial distribution of observations are not sufficient to adequately determine the location of the isoseismals and the $A_{(MMI)}$. In addition, isoseismal lines for many California earthquakes extend into the Pacific Ocean so that the $A_{(MMI)}$ must be estimated by assuming symmetry. Finally, because the $A_{(MMI)}$ are an aggregation of the intensity data, the details and circumstances of the individual observations are obscured. Instead, following Evernden et al. (1981), we seek to determine earthquake source parameters from the individual intensity observations themselves. Furthermore, we tailor our procedures to be particularly appropriate for the analysis of the sparse intensity data sets available for pre-1900 California earthquakes.

Training-Set Earthquakes

Twenty-two recent California earthquakes west of the Sierra Nevada were selected to characterize the spatial distribution of intensities [Table 1a, Training Set]. The selected earthquakes occurred primarily in central California but include two large southern California earthquakes, the 1971 San Fernando earthquake and the 1994 Northridge earthquake (Fig. 1). Twelve strike- and oblique-slip sources, nine thrust-fault sources, and one normal-faulting source are included. Focal depths range from 2 to 18 km, but the depth ranges of significant source slip probably overlap for the $M > 5.5$ events. We use moment magnitude M (Hanks and Kanamori, 1979) as the reference magnitude; these are available for all but the four smallest ($M_L < 5$) training-set earthquakes. Since M and M_L are in good agreement on average

for $M_L < 6$ earthquakes (see Table 1), we use M_L as a surrogate for M for those four events.

Intensity Data from *United States Earthquakes*

Descriptions of all reported felt earthquakes in the United States were published annually from 1928 to 1986 in *United States Earthquakes*. The California Division of Mines and Geology (CDMG) has compiled descriptions of reported pre-1950 felt earthquakes in California (Toppozada *et al.*, 1981). *United States Earthquakes* since 1931 and the CDMG compilations assign intensity values where possible according to descriptions listed in the Modified Mercalli intensity scale of 1931 (MMI) proposed by Wood and Neumann (1931).

Table 1
Earthquake Sources

Event Name	Yr	Mo	Day	Hr:Min	Epi. (°N)	Epi. (°W)	Depth (km)	M_L	M	Mechanism	Reference
(a) Training Set											
Loma Prieta	1989	10	18	0:04	37.04	121.88	17.0	6.9	6.9	oblique thrust	No. Ca. Eqk. Data Ctr.
San Fernando	1971	2	9	14:00	34.41	118.40	8.4	6.4	6.7	thrust	Ellsworth (1990)
Northridge	1994	1	17	12:30	34.21	118.54	18.0	6.7	6.7	thrust	So. Ca. Data Ctr.
Coalinga 1	1983	5	2	23:42	36.23	120.32	10.0	6.7	6.5	thrust	**
Morgan Hill 1	1984	4	24	21:15	37.31	121.68	8.4	6.2	6.2	strike slip	Ellsworth (1990)
Parkfield 66	1966	6	28	4:26	35.95	120.50	8.0	5.7	6.1	strike slip	Ellsworth (1990)
Coalinga 2	1983	7	22	2:39	36.24	120.41	7.4	6.0	5.9	thrust	**
Oroville	1975	8	1	20:20	39.45	121.54	5.5	5.7	5.8	normal	No. Ca. Eqk. Data Ctr.
Livermore 1	1980	1	24	19:00	37.83	121.77	11.9	5.5	5.8	strike slip	Bolt *et al.* (1981)
Coyote Lake	1979	8	6	17:05	37.10	121.51	9.6	5.8	5.7	strike slip	Ellsworth (1990)
Mt. Lewis	1986	3	31	11:55	37.48	121.68	8.3	5.7	5.6	strike slip	No. Ca. Eqk. Data Ctr.
Coalinga 4	1983	6	11	3:09	36.26	120.45	2.4	5.2	5.4	thrust	**
Livermore 2	1980	1	27	2:33	37.75	121.70	12.4	5.6	5.4	strike slip	Bolt *et al.* (1981)
Coalinga 3	1983	7	25	22:31	36.23	120.40	8.4	5.3	5.2	thrust	**
Coalinga 7	1983	7	9	7:40	36.25	120.40	9.0	5.4	5.2	thrust	**
Coalinga 5	1983	5	9	2:49	36.25	120.30	12.0	5.3	5.1	thrust	**
Parkfield 75	1975	9	13	21:20	36.00	120.54	11.6	4.8		strike slip	No. Ca. Eqk. Data Ctr.
Coalinga 6	1983	5	24	9:02	36.25	120.32	8.9	4.7	4.7	thrust	**
Morgan Hill 2	1984	9	26	20:46	37.34	121.70	7.9	4.5	4.7	strike slip	No. Ca. Eqk. Data Ctr.
Halls Valley	1979	5	8	5:11	37.29	121.66	7.4	4.7		strike slip	No. Ca. Eqk. Data Ctr.
Alum Rock	1981	1	15	12:47	37.37	121.73	9.4	4.6		strike slip	No. Ca. Eqk. Data Ctr.
Pacifica	1979	4	28	0:44	37.65	122.47	12.9	4.4		strike slip	Uhrhammer (1981)
(b) Test Set											
Chalfant	1986	7	21	14:42	37.54	118.44	9.1	6.5	6.4	strike slip	Ellsworth (1990)
Kettleman Hills	1985	8	4	12:01	36.13	120.17	11	5.6	6.1	thrust	Ellsworth (1990)
Truckee	1966	9	12	4:41	39.42	120.16	10.0	6.0	5.9	strike slip	Ellsworth (1990)
Parkfield 1881*	1881	2	2	0:11	35.95	120.50				strike slip	Bakun and McEvilly (1984)
Parkfield 01†	1901	3	3	7:45	35.95	120.50				strike slip	Bakun and McEvilly (1984)
Parkfield 22‡	1922	3	10	11:21	35.95	120.50			6.1	strike slip	Bakun and McEvilly (1984)
Parkfield 34‡	1934	6	8	4:47	35.95	120.50		5.6	6.1	strike slip	Bakun and McEvilly (1984)
Santa Rosa	1969	10	2	§	38.47	122.72		§		strike slip	Wong and Bolt (1995)
Petrolia	1986	11	21	23:33	40.33	124.44	15	5.1	5.2	strike slip	Stover and Brewer (1994)

*Probable ground rupture of the San Andreas fault southwest fracture zone where rupture occurred in 1966 (Toppozada, written comm., 1985).
**Bennett and Sherburne (1983); Rymer and Ellsworth (1990).
†$M_S = 6.4 \pm 0.2$ (Abe, 1988). Assume 1966 epicenter, although surface rupture likely extended northwest of the 1966 zone (Real, 1985).
‡M for 1922 $= M$ for 1934 $= M$ for 1966/1.2. Data are consistent with coincident 1922, 1934, and 1966 epicenters.
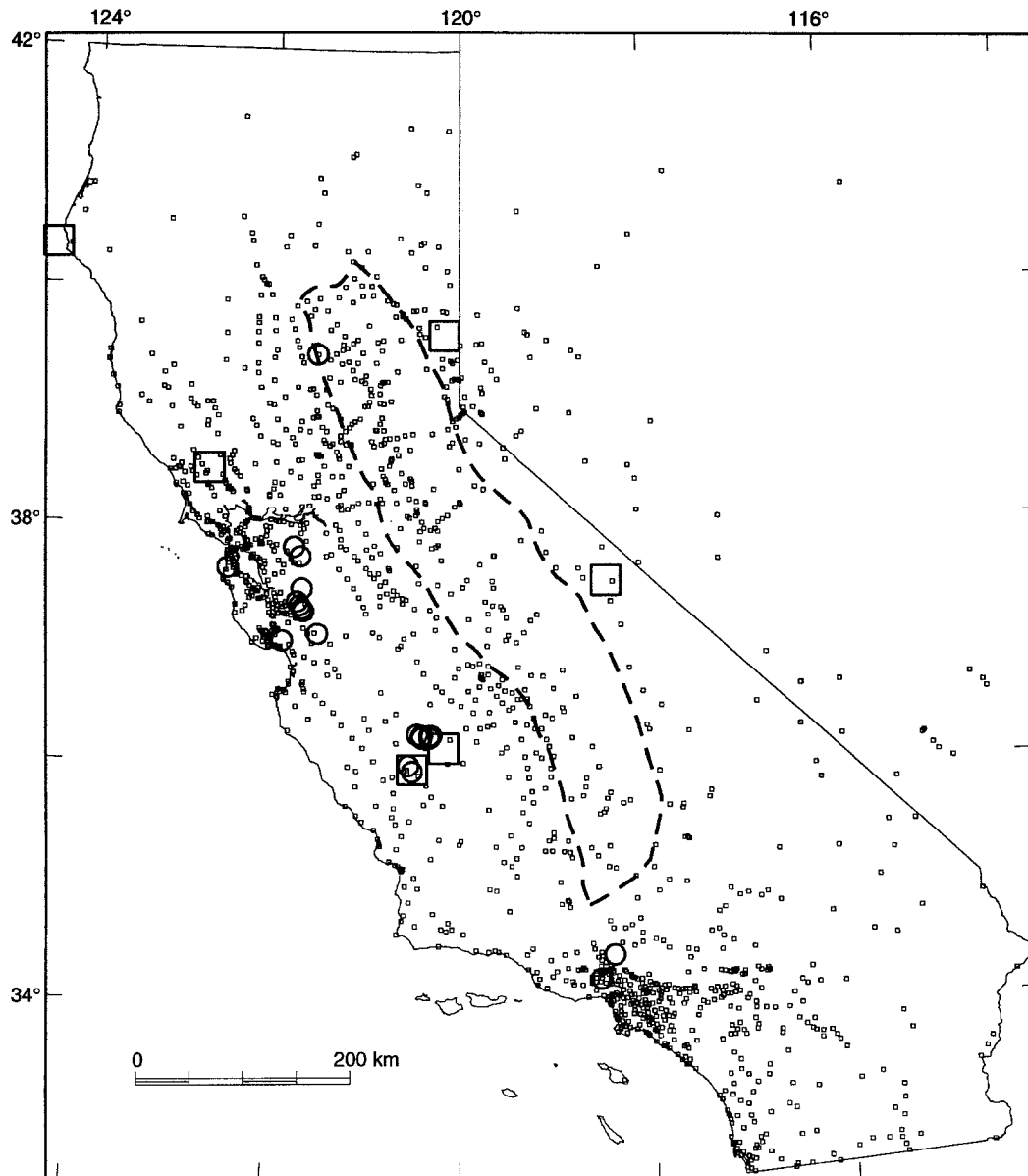§Two events: $M_L = 5.6$ at 04:56:46 and $M_L = 5.7$ at 06:19:57.

Figure 1. Map showing epicenter locations of the 22 training-set earthquakes (*circles*), the 9 test-set earthquakes (*boxes*, 4 at Parkfield), and the 1429 California and Nevada MMI sites. Dashed line bounds crystalline rocks of the Sierra Nevada, east of which lies the Basin and Range tectonic province.

We have assembled a data set of intensity observations and their geographic locations from several sources and then modified it to avoid ambiguity and inconsistency. Maps of intensities and lists of geographic names and assigned intensity values for locations where earthquakes were reported as felt are contained in the yearly issues of *United States Earthquakes* (Neumann, 1936; von Hake and Cloud, 1968, 1971; Coffman and von Hake, 1984; Coffman and Stover, 1984; Stover and von Hake, 1982, 1984; Stover, 1984; 1987, 1988; Stover and Brewer, 1991, 1994). Intensity data for the 1989 Loma Prieta and the 1994 Northridge earthquakes are in Stover *et al.* (1990) and Dewey *et al.* (1995), respectively.

Some modifications of the intensities assigned in *United States Earthquakes* were made for this study. Since many of the effects that are used to assign MMI X and larger are ground-failure or surface-faulting phenomena and may not be well correlated with shaking phenomena used for assigning lower intensities, we have reduced the MMI X and XI values assigned for the 1971 San Fernando earthquake to MMI IX. (The San Fernando shock was the only training-set event with MMI X or XI assigned by NEIS.) Since the descriptions for MMI I, II, and III are difficult to differentiate in practice, MMI I and MMI II observations were changed to MMI III. *United States Earthquakes* contains geographic

names under a "Felt" listing, implying inconsistent or ambiguous accounts; such Felt data points were excluded. Similarly, "Not Felt" data points were excluded. For a given earthquake, some geographic names are listed more than once in *United States Earthquakes;* all such conflicting intensity data were excluded. Finally, only MMI reported for locations in California and Nevada were used in this study.

The intensity data were examined for potential ambiguities and to standardize the association of geographic coordinates with geographic names through a gazetteer compiled by merging the current USGS/NEIC gazetteer for California and Nevada, the USGS Geographic Names Information System (GNIS) for California (U.S. Geological Survey, 1995), and the coordinates for Nevada geographic names assigned for the 1989 Loma Prieta earthquake by USGS/NEIC. USGS/NEIC gazetteer entries were deleted if a GNIS entry had the same geographic name and a location within 3 km. For Nevada geographic names, USGS/NEIC gazetteer entries were deleted if a Loma Prieta USGS/NEIC entry had the same geographic name and a location within 3 km.

Many geographic names in the merged gazetteer are listed more than once with different locations, making uncertain the assignment of correct locations to the intensity observations. All intensity observations with a geographic name having three or more potential geographic locations were deleted. There are a few geographic names with two locations so close together that it would be easy to use the wrong location; these intensity values were also deleted. The resulting merged gazetteer was then used to assign locations to each remaining geographic name in the MMI data such that the same location was associated with a geographic place name for all of the earthquakes in Table 1.

The resulting data set (hereafter called *the MMI data*) contains 4344 intensity values (see Table 2) recorded at 1253 geographic locations. Number of observations at a location (*hits*) range from 1 at 470 sites to 15 at 2 sites. Most of the MMI IX and MMI VIII observations were reported at sites with only one or two hits. These characteristics reflect the common practice in *United States Earthquakes* of specifying the locations of extraordinary or spectacular localized damage by neighborhood or district within a town. *United States Earthquakes* tends to associate unnoteworthy intensities with larger geographic entities (entire towns), for which intensity data are more likely to be available for a number of earthquakes.

Analysis

Intensity data are determined by the earthquake source, the propagation path between source and receiver, upper crustal structure near the observation site, site amplification, and recorder response. Parameters of the earthquake source include moment magnitude **M**, epicenter location, the location and length of the rupture plane, source directivity, moment centroid, stress drop, and source mechanism. Propa-

Table 2
Intensity Data—Number of Observations

Event Name	MMI III	MMI IV	MMI V	MMI VI	MMI VII	MMI VIII	MMI IX	Total
(a) Training Set								
Loma Prieta	115	136	103	97	79	25	5	560
San Fernando	39	88	256	87	31	3	2	506
Northridge	36	123	172	51	23	24	9	438
Coalinga 1	125	157	129	16	1	2		430
Morgan Hill 1	103	119	140	20	3			385
Parkfield 66	40	77	39	14	2			172
Coalinga 2	81	86	24	3				194
Oroville	81	96	99	15	3			294
Livermore 1	72	114	43	21	1			251
Coyote Lake	70	116	52	8	4			250
Mt. Lewis	38	88	43	4				173
Coalinga 4	20	6	2	1				29
Livermore 2	11	44	18	11	2			86
Coalinga 3	55	20	5	1				81
Coalinga 7	17	22	4					43
Coalinga 5	75	57	13	1				146
Coalinga 6	8	8	2					18
Morgan Hill 2	22	10	2					34
Parkfield 75	20	8	9	1				38
Halls Valley	37	46	5					88
Alum Rock	19	47	9					75
Pacifica	31	19	3					53
Total	1115	1487	1172	351	149	54	16	4344
(b) Test Set								
Chalfant	64	95	29	2				190
Kettleman Hills	35	100	32	2				169
Truckee	47	102	106	44	10			309
Parkfield 81	*	*	*	*		1		7
Parkfield 01	3		1	4		2		10
Parkfield 22	3	4	4		3			14
Parkfield 34	37	40	13	3	2	2		97
Santa Rosa	21	44	95	8		2		170
Petrolla	12	12	10	6	1			41
Total	222	397	290	69	16	7	0	1007

*Toppozada *et al.* (1981). See text for interpretation of damage descriptions.

gation path effects might include geometrical spreading, attenuation and scattering, and reflections from Moho and lower crustal interfaces. Effects of upper crustal structure might include trapped and guided waves within and near basins. Site amplification might result from material properties of the site geology, topography, depth to water table, and soil saturation (rainy versus dry season). "Recorder response" for intensity data includes the differences in the sensitivity of people and man-made structures to ground motions. While it should be possible to quantify the contribution of these effects using the comparatively large data sets available for recent earthquakes, we focus in this study on the development of procedures for estimating source location and moment magnitude **M** with a minimum of free parameters appropriate to the sparse intensity data available for pre-1900 earthquakes.

Analyses of high-fidelity ground-motion data agree that the steps in intensity vary with parameters of strong ground motion, although there is continuing evaluation of the relative merits of competing empirical functions that relate ground-motion parameters and earthquake intensity. These analyses generally demonstrate that the amplitude and duration of strong shaking at frequencies that damage man-made structures are affected significantly by distance from the source and by the physical characteristics of soils beneath the recording site. In fact, detailed geology is an important component in earthquake hazard models of strong ground motion (e.g., Borcherdt *et al.*, 1991). These attributes of intensity—the strictly empirical relation of intensity to quantitative seismology, and the importance of epicentral distance and local geology for the satisfactory prediction of strong shaking, and therefore presumeably for intensity—figure in our strategy to develop a robust method for estimating earthquake source parameters from intensity data alone.

The importance of site conditions, including local geology, in modeling historic intensity data is obvious. The maps of intensity published in *United States Earthquakes* clearly show pockets of anomalously high intensities where communities are built on soft soils. For example, parts of San Francisco built on nonengineered landfill and natural soft soils have consistently experienced greater effects from near and regional earthquakes than have other areas at comparable distance. Although clearly important, the details of local geology are unknown for all but a very small fraction of historic intensity observations. Usually the name of the community and the descriptive account of the earthquake effects are all that is known. If the community is larger than the spatial variations of local geology (as it nearly always is in western California), there is no way to recover what particular site or sites in the community, and what particular geology or other site conditions, should be matched with the intensity value assigned for that community.

Our objective is a robust procedure for using intensity data to reliably estimate earthquake source parameters. We know site conditions are important, but there is no objective *a priori* way to identify those intensity observations particularly affected by site conditions. Ignoring site conditions and weighting all of the intensity observations equally in the analysis effectively overemphasizes anomalous intensity observations that often can be rationalized as the effect of anomalous site conditions. Our experience is that the resulting relationships provide poor estimates of the desired source parameters. Rather than a fit to the intensity data where outliers are implicitly emphasized, we will seek the best fit to the central tendencies of the intensity data; deviations from those central tendencies then can be partially accounted for through site corrections. Site corrections in this context will play a role familiar to seismologists—that of station corrections in the definition and application of a magnitude scale such as M_L. Ideally, the empirical site corrections will be correlated to those site conditions, such as

local geology, known to affect ground motions significantly. The central tendency that we will fit is the median epicentral distance of an intensity step value for a training set of recent California earthquakes. The relationship obtained from this fit to the median distance will then be applied to individual intensity observations at their epicentral distances. Testing the relationship on the training set itself and then on an independent test set of earthquakes will demonstrate that the relationship provides a remarkably robust and reliable measure of seismic moment and spatial bounds of the epicentral region for northern California earthquakes west of the Sierra Nevada.

Source-Receiver Distance and Magnitude

The distribution of epicentral distances Δ for the 22 training-set earthquakes is concentrated in the 0- to 150-km range (see Fig. 2) reflecting the proximity of the epicenters to the population centers of coastal California. The distributions of intensity observations with epicentral distance for eight of the earthquakes spanning the $4.4 \leq M \leq 6.9$ range are shown in Figure 3. Epicentral distances for each intensity unit range over hundreds of kilometers, and the ranges for adjacent intensity values overlap conspicuously. The distribution of epicentral distance for an intensity value is typically skewed, with outliers at large distance for each intensity value. Mean and median distances and standard deviations were computed for each event and intensity after excluding data at epicentral distances greater than ± 2 standard deviations. The resulting median epicentral distances are fit well by linear trends (*dashed lines* in Fig. 3), although MMI IX observations (the Loma Prieta, Northridge, and San Fernando earthquakes) all lie at greater epicentral distance than predicted by the linear trends. Using distance from the rupture plane (e.g., Evernden, 1975) would reduce this discrepancy, but not eliminate it. The five MMI IX observations for the Loma Prieta earthquake at $\Delta = 93$ to 98 km reflect damaged freeways in Oakland and San Francisco and significant damage in the Marina district of San Francisco. Such
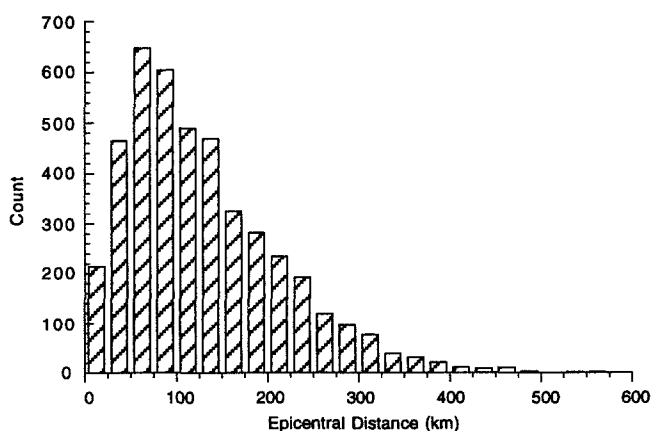

Figure 2. Distribution of epicentral distances for the 22 training-set earthquakes.
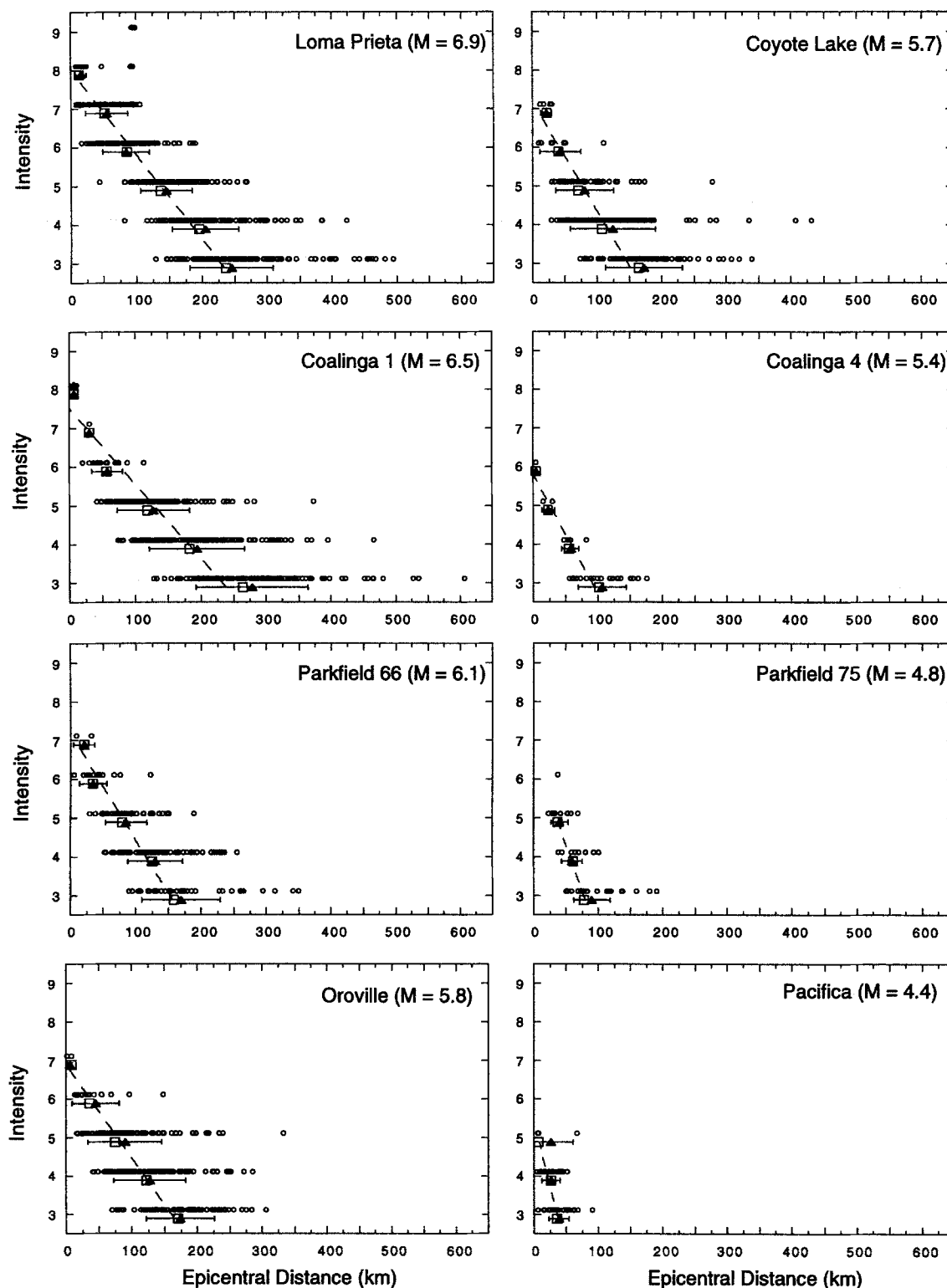
Figure 3.   Intensity versus epicentral distance. Circles represent individual intensity values. Mean and median epicentral distance for each intensity-source pair, computed without outliers (distance more than 2 standard deviations from the mean distance), are solid diamonds and open squares, respectively. Error bars are ± 1 standard deviation of the data computed without outliers. The median distances are fit with least-squares straight lines (*dashed*). The intensity IX data for the Loma Prieta earthquake and the intensity VI data for the Parkfield 75 earthquake considered as outliers were not used in these fits.

distant structural failures result from special circumstances, in this case critical reflections from the base of the crust (Somerville and Yoshimura, 1990) combined with local site amplification and ground failure on poor ground.

The linear trends of MMI with median distance are summarized in Figure 4. The slopes of these trends increase with **M**, although slopes for the **M** < 5.5 earthquakes are poorly determined, and the slopes for the **M** > 5.5 earthquakes are nearly constant. For simplicity, we will assume a constant slope; that is, the decrease of intensity with distance is the same for all magnitudes and distances. Intercepts increase nearly linearly over the 4.4 ≤ **M** ≤ 6.9 magnitude range, but again the intercepts for the **M** < 5.5 earthquakes are poorly determined. Constant slope and a linear increase of intercept with **M** suggest the functional relation

$$\text{MMI} = c_0 + c_1 * \mathbf{M} + c_2 * (\text{median } \Delta). \qquad (1)$$

We also evaluate

$$\text{MMI} = c_0 + c_1 * \mathbf{M} + c_2 * \log_{10} (\text{median } \Delta), \qquad (2)$$

which allows for the nonlinear character noted above for the high intensities of the largest earthquakes.

The change in the quality and consistency of the slopes and intercepts at **M** = 5.5 suggest fitting the above functional relations with the 11 **M** > 5.5 events separately as well as with all twenty-two 4.4 ≤ **M** ≤ 6.9 events. Linear least-squares fits using all the median Δ, except that for Loma Prieta MMI IX, resulted in the following relations.

For the twenty-two 4.4 ≤ **M** ≤ 6.9 events,

$$\text{MMI} = -1.72 + 1.44 * \mathbf{M} - 0.0212 * (\text{median } \Delta), \qquad (3)$$

and

$$\text{MMI} = 3.67 + 1.17 * \mathbf{M} - 3.19 * \log_{10} (\text{median } \Delta). \qquad (4)$$

For the 11 **M** > 5.5 events,

$$\text{MMI} = -3.29 + 1.68 * \mathbf{M} - 0.0206 * (\text{median } \Delta), \qquad (5)$$

and

$$\text{MMI} = 5.07 + 1.09 * \mathbf{M} - 3.69 * \log_{10} (\text{median } \Delta). \qquad (6)$$

Although these relations were obtained from fits of median Δ, they will be used to estimate **M** from individual intensity observations. We define $\mathbf{M}_i^{(j)}$ to be an estimate of **M** determined from an intensity observation MMI_i at Δ_i using relation j. That is,

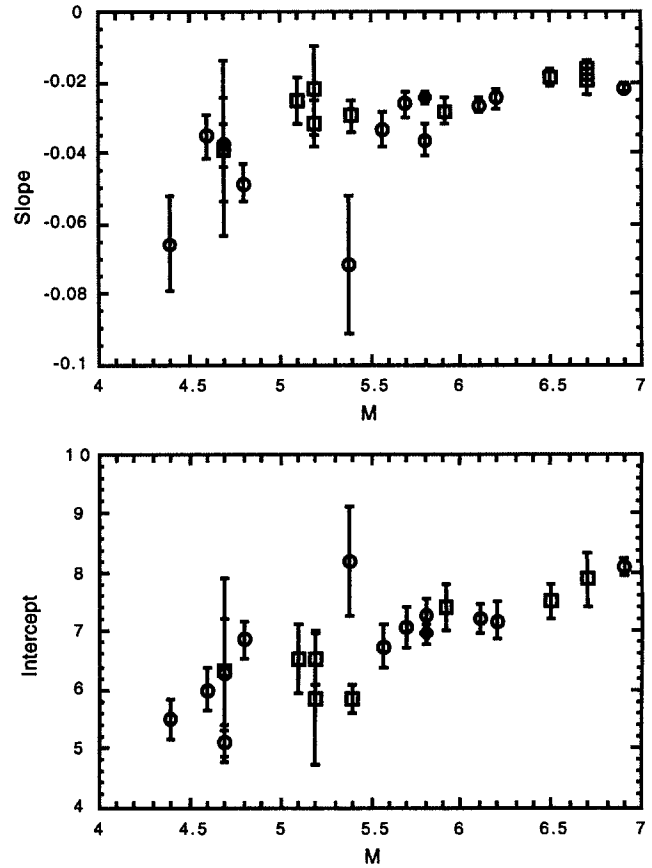$$\mathbf{M}_i^{(1)} = (\text{MMI}_i + 1.72 + 0.0212 * \Delta_i)/1.44. \qquad (7)$$

Figure 4. Slopes and intercepts of least-squares fits of MMI = $a + b *$ median distance (see Fig. 3). Strike-slip (including Loma Prieta), thrust, and normal focal mechanism sources shown as circles, squares, and diamonds, respectively. Error bars are 1 standard error.

$$\mathbf{M}_i^{(2)} = [\text{MMI}_i - 3.67 + 3.19 * \log_{10} (\Delta_i)]/1.17. \qquad (8)$$

$$\mathbf{M}_i^{(3)} = (\text{MMI}_i + 3.29 + 0.0206 * \Delta_i)/1.68. \qquad (9)$$

$$\mathbf{M}_i^{(4)} = [\text{MMI}_i - 5.07 + 3.69 * \log_{10} (\Delta_i)]/1.09. \qquad (10)$$

We define $\mathbf{M}_I$ to be the mean $(\mathbf{M}_i)$. That is,

$$\mathbf{M}_I^{(1)} = \text{mean } (\mathbf{M}_i^{(1)}), \qquad (11)$$

$$\mathbf{M}_I^{(2)} = \text{mean } (\mathbf{M}_i^{(2)}), \qquad (12)$$

$$\mathbf{M}_I^{(3)} = \text{mean } (\mathbf{M}_i^{(3)}), \qquad (13)$$

$$\mathbf{M}_I^{(4)} = \text{mean } (\mathbf{M}_i^{(4)}). \qquad (14)$$

$\mathbf{M}_I^{(1)}, \mathbf{M}_I^{(2)}, \mathbf{M}_I^{(3)},$ and $\mathbf{M}_I^{(4)}$ for the training-set events are listed in Table 3 and plotted in Figure 5. $\mathbf{M}_I^{(1)}$ and $\mathbf{M}_I^{(3)}$ provide comparable fits for **M** < 5.5, and each is better than $\mathbf{M}_I^{(2)}$ and $\mathbf{M}_I^{(4)}$ for these smaller events. $\mathbf{M}_I^{(2)}, \mathbf{M}_I^{(3)},$ and $\mathbf{M}_I^{(4)}$ pro-

vide comparable fits for $\mathbf{M} > 5.5$, and each is better than $\mathbf{M}_f^{(1)}$ for these larger events.

Site Corrections and Site Amplification

Site corrections were calculated independently for $\mathbf{M}_f^{(1)}$, $\mathbf{M}_f^{(2)}$, $\mathbf{M}_f^{(3)}$, and $\mathbf{M}_f^{(4)}$ for each reporting site. A *site correction* is the mean {observed MMI − calculated intensity} at a reporting site for all training-set earthquakes. Site corrections are additive amplification factors in the sense that they are the increment to be subtracted from the observed intensity to account for amplification at a site. Note that this definition of site correction implicitly assumes a linearity in the MMI scale in the sense that site conditions increment intensity uniformly (e.g., site conditions incrementing MMI III to IV will increment MMI VIII to IX). Applying site corrections reduces the skewness and outliers in the distributions of $\mathbf{M}_I$ (Fig. 6).

The estimates of $\mathbf{M}$ obtained applying $\mathbf{M}_f^{(1)}$, $\mathbf{M}_f^{(2)}$, $\mathbf{M}_f^{(3)}$, and $\mathbf{M}_f^{(4)}$ to the intensity observations with site corrections are listed in Table 3. Applying site corrections generally reduces the mean $(\mathbf{M} - \mathbf{M}_f^{(p)})$ and the rms $(\mathbf{M} - \mathbf{M}_f^{(p)})$ for the training-set events. Comparisons of the rms $(\mathbf{M} - \mathbf{M}_f^{(p)})$ in Table 3 show that $\mathbf{M}_f^{(3)}$ is a better fit to $\mathbf{M}$ than $\mathbf{M}_f^{(1)}$, $\mathbf{M}_f^{(2)}$, or $\mathbf{M}_f^{(4)}$. Hereafter we restrict our discussion to $\mathbf{M}_f^{(3)}$ and simplify the notation:

$$\mathbf{M}_i = \mathbf{M}_i^{(3)} \tag{15}$$

and

$$\mathbf{M}_I = \mathbf{M}_f^{(3)}. \tag{16}$$

For $\mathbf{M} > 5.5$, rms $[\mathbf{M} - \mathbf{M}_I]$ is reduced from 0.16 to 0.13 with site corrections; rms $[\mathbf{M} - \mathbf{M}_I]$ for $\mathbf{M} < 5.5$ increases from 0.27 to 0.29 with site corrections. The rms $[\mathbf{M} - \mathbf{M}_I]$ = 0.13 is comparable to the uncertainty of $\mathbf{M}$ for the $\mathbf{M} > 5.5$ events, and the uncertainty of $\mathbf{M}$ for the $\mathbf{M} < 5.5$ events is larger. That is, the rms $[\mathbf{M} - \mathbf{M}_I]$ with site corrections might be explained as errors in the $\mathbf{M}$ used for the training-set events.

Local Geology

The importance of local geology in modeling strong ground motion data (e.g., Borcherdt *et al.*, 1991) suggests that local geology is a likely significant component of the empirical site corrections. In particular, ground-motion data are sensitive to the stiffness of the soils underlying the recording sites (e.g., see Borcherdt and Glassmoyer, 1994). Here we seek correlations between the empirical site corrections for intensity and attributes of the local geology. Our results will be conditioned by our necessary association of an MMI reported for a community to a single geographic

Table 3
Estimates of $\mathbf{M}$ Using Intensity Data

| Event Name | $\mathbf{M}_L$ | $\mathbf{M}$ | Without Site Corrections | | | | With Site Corrections | | | |
			$\mathbf{M}_f^{(1)}$	$\mathbf{M}_f^{(2)}$	$\mathbf{M}_I = \mathbf{M}_f^{(3)}$	$\mathbf{M}_f^{(4)}$	$\mathbf{M}_f^{(1)}$	$\mathbf{M}_f^{(2)}$	$\mathbf{M}_I = \mathbf{M}_f^{(3)}$	$\mathbf{M}_f^{(4)}$
Loma Prieta	6.9	6.9	6.97	6.77	6.84	6.93	6.92	6.75	6.81	6.92
San Fernando	6.4	6.7	6.88	6.76	6.77	6.91	6.90	6.77	6.78	6.92
Northridge	6.7	6.7	6.68	6.56	6.60	6.66	6.66	6.52	6.59	6.63
Coalinga 1	6.7	6.5	6.88	6.42	6.76	6.62	6.76	6.43	6.67	6.62
Morgan Hill 1	6.2	6.2	6.04	5.99	6.06	6.07	6.04	6.00	6.08	6.08
Parkfield 66	5.7	6.1	5.96	5.95	5.99	6.03	5.99	5.96	6.01	6.03
Coalinga 2	6.0	5.9	5.87	5.76	5.91	5.86	5.82	5.71	5.88	5.78
Oroville	5.7	5.8	5.91	5.90	5.95	5.96	5.93	6.03	5.97	6.09
Livermore 1	5.5	5.8	5.48	5.55	5.59	5.55	5.51	5.55	5.64	5.55
Coyote Lake	5.8	5.7	5.84	5.82	5.89	5.89	5.82	5.79	5.88	5.85
Mt. Lewis	5.7	5.6	5.24	5.41	5.39	5.37	5.34	5.40	5.50	5.37
Coalinga 4	5.2	5.4	4.88	4.86	5.08	4.78	4.87	4.87	5.03	4.66
Livermore 2	5.6	5.4	5.07	5.25	5.26	5.13	5.21	5.26	5.43	5.19
Coalinga 3	5.3	5.2	4.96	5.05	5.15	5.03	5.04	5.06	5.23	5.02
Coalinga 7	5.4	5.2	5.26	5.33	5.40	5.33	5.33	5.33	5.50	5.35
Coalinga 5	5.3	5.1	5.48	5.44	5.58	5.48	5.47	5.42	5.62	5.45
Parkfield 75	4.8		4.99	5.10	5.17	5.04	5.04	5.11	5.20	4.99
Coalinga 6	4.7	4.7	4.67	4.72	4.91	4.58	4.84	4.84	5.04	4.70
Morgan Hill 2	4.5	4.7	4.32	4.24	4.61	4.03	4.56	4.39	4.87	4.30
Halls Valley	4.7		4.85	4.96	5.06	4.88	4.96	4.92	5.20	4.88
Alum Rock	4.6		4.88	4.96	5.09	4.85	5.02	4.98	5.26	4.94
Pacifica	4.4		4.12	3.78	4.45	3.45	4.19	3.67	4.56	3.32
mean $[\mathbf{M} - \mathbf{M}_f^{(p)}]$, $\mathbf{M} < 5.5$			0.06	0.04	−0.14	0.15	−0.03	0.03	−0.25	0.13
rms $[\mathbf{M} - \mathbf{M}_f^{(p)}]$, $\mathbf{M} < 5.5$			0.30	0.36	0.27	0.44	0.29	0.37	0.29	0.46
mean $[\mathbf{M} - \mathbf{M}_f^{(p)}]$, $\mathbf{M} > 5.5$			0.01	0.09	0.02	0.00	0.02	0.09	0.01	0.01
rms $[\mathbf{M} - \mathbf{M}_f^{(p)}]$, $\mathbf{M} > 5.5$			0.22	0.13	0.16	0.16	0.18	0.15	0.13	0.18
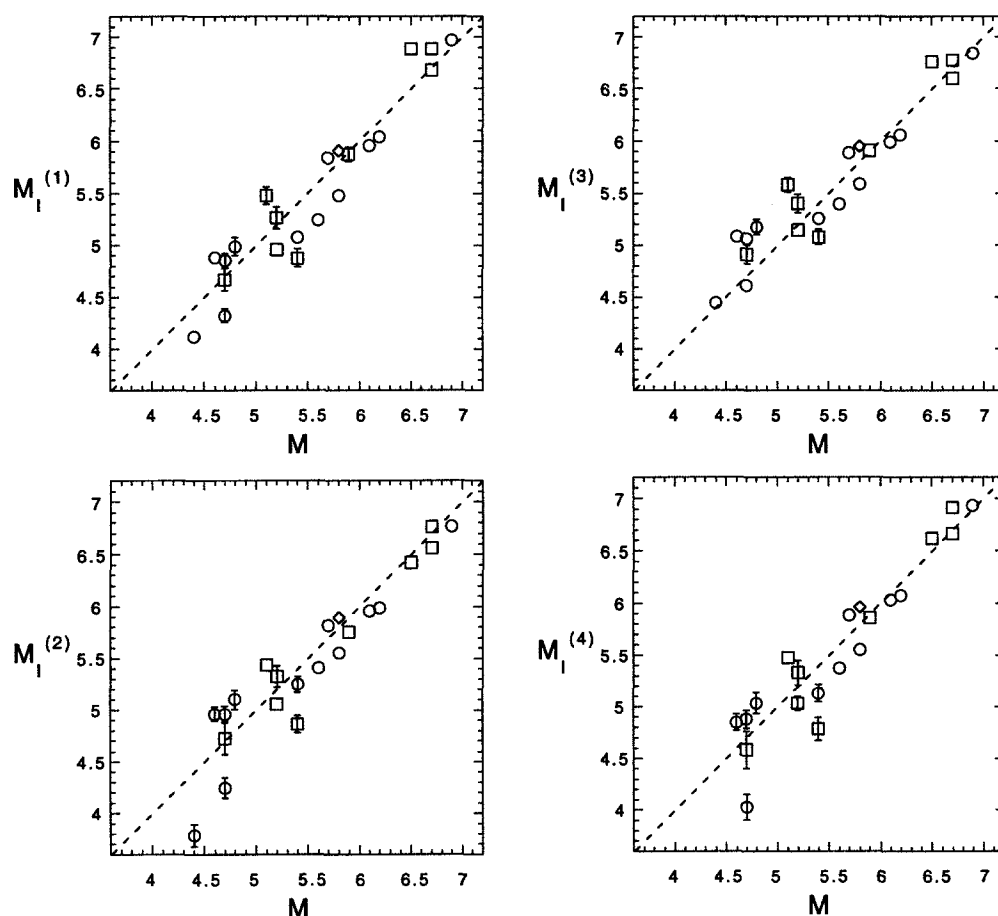
Figure 5. $M_I^{(j)}$ versus M for training-set earthquakes. Strike-slip (including Loma Prieta), thrust, and normal focal mechanism sources shown as circles, squares, and diamonds, respectively. Error bars are 1 standard error of $M_I^{(j)}$; error bars not shown if standard error less than 0.065. Dashed line is $M_I^{(j)} = M$.

coordinate within that community and its associated geology; since many of the communities listed in *United States Earthquakes* occupy relatively large areas, the geologic unit at the point location may have little relation to the geology underlying the unspecified sites critical in assigning the MMI value to that community.

Surface geologic materials in the region range from soft, water-saturated mud to hard granitic rock. To the extent that intensity varies with ground motion, the local geology at each reporting site should affect the reported intensities and the site corrections. Two available digital data sets, the geologic map of California and a subdivision of geologic materials into soil classes in the southern San Francisco Bay region, were used to explore the influence of local ground conditions on the intensity ratings.

A working digital version of the geologic map of California (Jennings, 1977) covers the whole state at a scale of 1:750,000. Six categories were aggregated from the generalized units of the map based largely on age (sedimentary rocks in California generally increase in stiffness or hardness with age):

CA 1. Older sedimentary and all volcanic, plutonic, and metamorphic rocks.

CA 2. Lower Tertiary sedimentary rocks.

CA 3. Miocene sedimentary rocks.

CA 4. Pliocene sedimentary rocks.

CA 5. Plio-Quaternary, semi-consolidated sandstone, shale, and gravel.

CA 6. Quaternary surficial deposits.

Most surficial deposits are included in a single unit on this map (Q, consisting of unconsolidated and semiconsolidated alluvium, lake, playa, and terrace deposits).

A more detailed representation of geologic materials at 1:125,000 containing the Quaternary subdivisions of Helley and Lajoie (1979) provided subdivision of the surficial deposits as well as bedrock in the southern San Francisco Bay region (Wentworth, 1993). Four categories were aggregated from the many map units, based on working unit assignments (Roger Borcherdt and Carl Wentworth, written comm., 1996) to the new soil classes proposed for building-code provisions (Borcherdt, 1994):
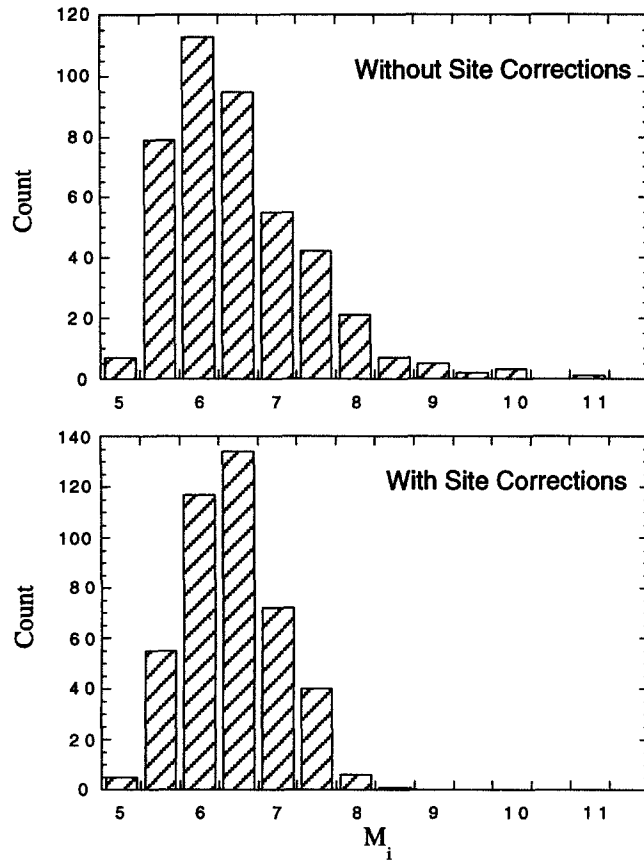
Figure 6. Distribution of $M_i = M_i^{(3)}$ from the 430 intensity observations from the Coalinga mainshock (Coalinga 1).

Table 4
Geologic/Soil-Based Site Corrections for M_I

Material Unit	Mean ± Std. Err.	Median	Std. Dev.	No. of Site Corr.
(a) California Geology				
CA 1	-0.08 ± 0.06	-0.25	1.10	313
CA 2	0.34 ± 0.24	0.00	1.30	30
CA 3	-0.36 ± 0.12	-0.46	0.76	43
CA 4	0.29 ± 0.39	-0.02	1.78	21
CA 5	-0.24 ± 0.12	-0.18	0.66	31
CA 6	-0.05 ± 0.04	-0.16	1.09	862
(b) Southern San Francisco Bay Region Soils				
SC I	-0.39 ± 0.11	-0.38	0.68	41
SC II	-0.49 ± 0.17	-0.40	0.46	7
SC III	-0.32 ± 0.07	-0.40	0.74	107
SC IV	0.72 ± 0.29	0.45	1.32	20

soft to very soft soils have more-than-predicted intensity (large positive site corrections for SC IV). Unfortunately, geologic data are not yet available to make such distinctions throughout the study area.

Resolution of the Epicentral Region

The preceding analysis assumes that earthquake epicenters are known. In fact, the epicentral regions of pre-1900 earthquakes are not known except in the few cases where surface faulting is documented. If an assumed epicenter located outside the actual epicentral region is used, the calculated epicentral distances and resulting M_i are biased. While the biases in M_i tend to cancel in the mean, the M_I differ by up to 0.25 if the assumed epicenter is located a few tens of kilometers from the instrumental epicenter (Figs. 7a and 7b). Note that the minimum in M_I is located about 50 km east of the instrumental epicenter of the Northridge earthquake. Site corrections do not appear to significantly change the spatial patterns of M_I.

The equal weighting of intensity observations above implicitly assumes that all intensity observations are equally sensitive to source magnitude. In contrast, intensity observations near an assumed epicenter are particularly sensitive to an error in its location. This suggests that observations at near distances be preferentially weighted when using intensity data to resolve the epicentral region.

SC I. Firm and hard rock: shear-wave velocity $\beta > 700$ m/sec.

SC II. Gravelly soils and soft to firm rock: $\beta = 375$ to 700 m/sec.

SC III. Stiff clays and sandy soils: $\beta = 200$ to 375 m/sec.

SC IV. Soft soils, very soft to soft clays: $\beta = 100$ to 200 m/sec.

Based on the coordinates assigned to the geographic names, a geologic unit CA number was attributed to each reporting site and a soil class SC number was attributed to each site within the southern San Francisco Bay region. For example, the 10 observations reported for Daly City (geologic unit Ku, materials unit #656) were assigned CA = 1 and SC = I.

The relation of the site corrections for M_I on site geology is summarized in Table 4. The California geologic units apparently do not provide a basis for rationalizing the site corrections. In fact, the distributions of site corrections for the stiffest rocks (CA 1) and for Quaternary surficial deposits (CA 6) are indistinguishable. The southern San Francisco Bay soil units do, however, seem to provide a geologic basis for the variations in site corrections. Sites underlain by the stiffest material have less-than-predicted intensity (large negative site corrections for SC I), and the sites underlain by

$$\text{Let } W_i = \begin{cases} 0.1 + \cos\left[(\Delta_i/150) * \pi/2\right], & \text{for } \Delta_i < 150 \text{ km}, \\ 0.1, & \text{for } \Delta_i > 150 \text{ km}. \end{cases} \quad (17)$$

The choices of the cosine weighting function, the cutoff distance of 150 km, and the "water level" $W_i = 0.1$ are reasonable but arbitrary.

For each assumed epicenter, let

$$\text{rms } [M_I] = \text{rms } [M_I - M_i] - \text{rms}_0 [M_I - M_{ii}], \quad (18)$$
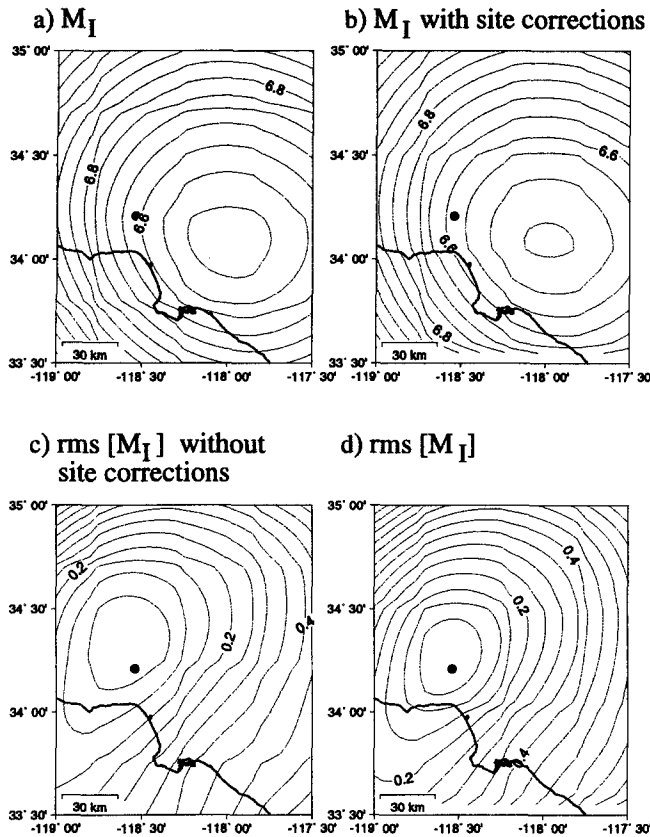
a) M_I

b) M_I with site corrections

c) rms [M_I] without site corrections

d) rms [M_I]

Figure 7.   Maps of contours of M_I in (a) and (b) and rms [M_I] in (c) and (d) as thin lines for the M = 6.7 Northridge earthquake for a 5-km-spaced grid of assumed epicenters. The contour interval is 0.05. California coastline is shown as a thick line. The solid circle is the instrumental epicenter of the Northridge earthquake.

where rms [$M_I - M_i$] = $\{\Sigma_i[W_i * (M_I - M_i)]^2/\Sigma_i W_i^2\}^{1/2}$ and rms_0 [$M_I - M_i$] is the minimum rms [$M_I - M_i$] over the grid of assumed epicenters and where M_i are calculated with site corrections.

Rms [M_I], where M_i are not calculated with site corrections, and rms [M_I] are shown for the Northridge earthquake in Figures 7c and 7d, respectively. Note that the region of minimum rms [M_I] coincides with the Northridge rupture zone, which extends from the instrumental epicenter about 25 km to the north (Wald et al., 1996), and that site corrections slightly improve the coincidence of rupture zone and the region of minimum rms [M_I]. Rms [M_I] for four other training-set events are shown in Figure 8. The region near the minimum rms [M_I] coincides with the rupture area for each of the 22 training-set events, and site corrections tend to improve the association of the minimum rms [M_I] and the rupture areas.

Resolution of the Epicentral Region—Sparse MMI Data

The training-set events can be used to define empirical confidence limits for resolution of the epicentral region that

can be applied to earlier events for which the only available information is a comparatively small number of MMI observations. By randomly sampling the training-set MMI data, we can simulate a sufficiently large number of training-set events with a given small quantity of MMI data to empirically define contour values of rms [M_I] for which the instrumental epicenter lies within the region bounded by the contour a given percentage of the time. For example, since all 22 of the training-set epicenters lie within or near the rms [M_I] = 0.05 contour (e.g., see Figs. 7d and 8), we can anticipate that for events with many MMI available and where a high level of confidence in the bounds of the epicentral region is desired, then the appropriate rms [M_I] contour bounding the region of potential epicenters will be about 0.05.

Contour values of rms [M_I] have been associated with confidence levels for 5, 7, 10, 15, 20, 25, 30, 40, 50, 60, 70, 80, 90, 100, 110, 120, 130, 150, and 170 MMI observations. For example, the contour values for 30 MMI are obtained by constructing 1000 sets of 30 randomly picked MMI data from each of the 11 M > 5.5 training-set events. For each set, $rms_{epi}(M_I - M_i)$ − rms_0 ($M_I - M_i$) was calculated for a 200 × 200 km grid (41 N–S points × 41 E–W points, 5-km spacing centered on the instrumental epicenter) of candidate epicenters, where $rms_{epi}(M_I)$ is rms [M_I] at the instrumental epicenter and rms_0 ($M_I - M_i$) is the minimum rms ($M_I - M_i$) over the grid of assumed epicenters. The 1000 [$rms_{epi}(M_I - M_i)$ − rms_0 ($M_I - M_i$)] provide a basis for assigning empirical confidence levels to contours for each event. For example, 950 of the 1000 [$rms_{epi}(M_I - M_i)$ − rms_0 ($M_I - M_i$)] for 30 MMI points from the Loma Prieta earthquake are less than 0.137; the rms[M_I] contour = 0.137 is thus an empirical 95% confidence-level parameter for 30 MMI points, in that the Loma Prieta instrumental epicenter lies within this contour for 95% of the randomly selected sets of 30 MMI points. The 95% confidence-level rms[M_I] contour values for 30 MMI for the 11 M > 5.5 training-set events are shown in Figure 9a. The contour values increase with M, but there is considerable scatter, particularly for the thrust-faulting sources. The increase in contour value with M is probably related to the extended rupture zones of larger shocks and the resulting complex spatial distributions of MMI. The ordered 11,000 [$rms_{epi}(M_I)$ − $rms_0(M_I)$] for the 11 M > 5.5 training-set events are used to define the contour values of rms [M_I] corresponding to different confidence levels. For example, the 95% confidence rms [M_I] contour value for 30 MMI is 0.156; in this conservative calculation, the Coalinga 1 and Coalinga 2 events contribute heavily to the 95% confidence contour value. In contrast, the average of the 11 95% contour values is 0.14. The distributions with M_I for other quantities of MMI are similar to that shown in Figure 9a but shifted toward higher (lower) contour values for less (more) MMI points. Confidence-level contour values for rms [M_I] for different quantities of MMI data determined in the same fashion are listed in Table 5a and plotted in Figure 9b.
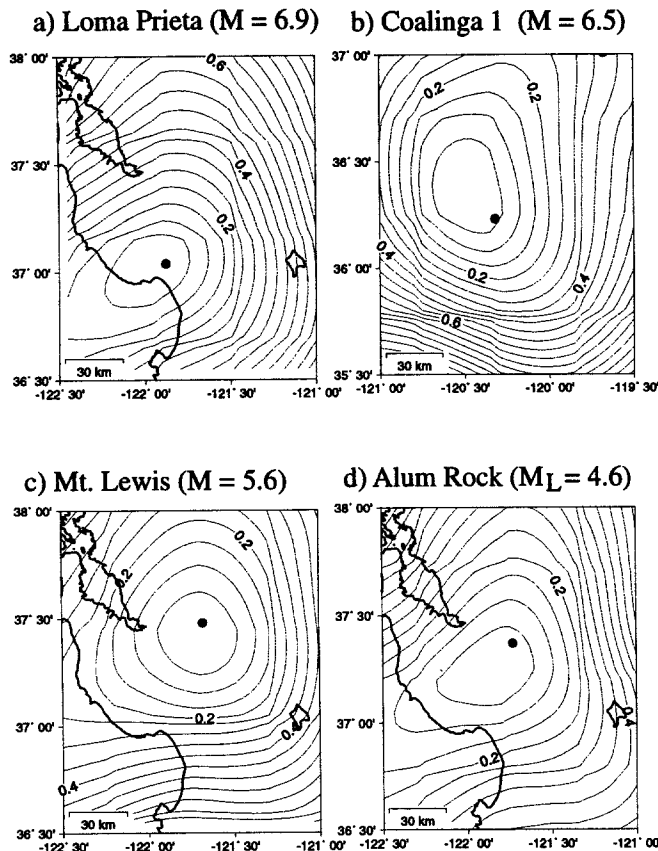
a) Loma Prieta (M = 6.9)   b) Coalinga 1 (M = 6.5)

c) Mt. Lewis (M = 5.6)   d) Alum Rock (M_L = 4.6)

Figure 8.   Maps of rms [$\mathbf{M}_I$] for (a) Loma Prieta, (b) Coalinga 1, (c) Mt. Lewis, and (d) Alum Rock earthquakes. Dots are the instrumental epicenters. See caption of Figure 7.

a) 30 MMI points

b) M_I > 5.5

Figure 9.   95% confidence-level contour values of rms [$\mathbf{M}_I$]: (a) for 30 MMI shown as dots, open squares, and open diamonds for strike slip (including Loma Prieta), thrust, and normal faulting training-set events, respectively; (b) for different quantities of MMI data.

Resolution of M—Sparse MMI Data

$\mathbf{M}_I$ varies slowly spatially for assumed epicenters and $\mathbf{M}_I$ is a good estimate of $\mathbf{M}$ for the numerous MMI available for the training-set events. How well is $\mathbf{M}_I$ resolved for sparse MMI data? More to the point, how well is $\mathbf{M}$ resolved by $\mathbf{M}_I$ calculated from sparse MMI data? Using randomly selected MMI data for each of the 11 $\mathbf{M} > 5.5$ training-set events, we calculated $\mathbf{M} - [\mathbf{M}_I]_{epi}$, where $[\mathbf{M}_I]_{epi}$ is $\mathbf{M}_I$ calculated using the set of randomly selected MMI data with site corrections and the instrumental epicenter. Following the method for the resolution of the epicentral region used above, the ordered 11,000 $\mathbf{M} - [\mathbf{M}_I]_{epi}$ are used to define confidence-level bounds for $\mathbf{M}$ estimated from $\mathbf{M}_I$ for different quantities of MMI data. The limits do not depend strongly on $\mathbf{M}$ (e.g., see the 95% confidence limits for 30 MMI in Fig. 10a). The limits for $\mathbf{M}$ for different confidence levels and different quantities of MMI data are listed in Table 5b. The limits for the 95% confidence level are shown in Figure 10b.

Strategy—Determination of Epicentral Region and M

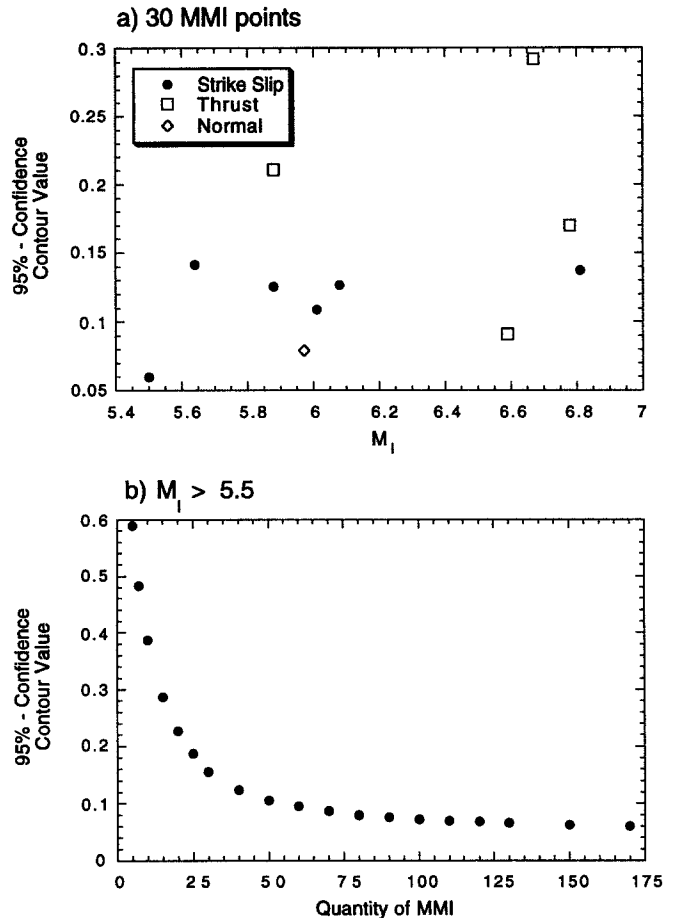The preceding suggests a strategy for the analysis of intensity data:

1. Calculate $\mathbf{M}_I$ and rms [$\mathbf{M}_I$] over a grid of trial epicenters.
2. The rms [$\mathbf{M}_I$] contours bound the epicentral region with levels of confidence appropriate for the quantity of MMI observations (Table 5a).
3. $\mathbf{M}_I$ at tectonically attractive trial epicenters within the appropriate confidence-level contours are the best estimates of $\mathbf{M}$ for those epicenters. The uncertainty in $\mathbf{M}$ appropriate for the quantity of MMI observations and the desired level of confidence is obtained from Table 5b.

Test-Set Earthquakes

The strategy for determining epicentral region and $\mathbf{M}$ suggested above is tested using three post-1965 western California, four earlier Parkfield, and two Basin and Range earthquakes [Table 1b Test Set]. Intensity data for the test-set events in *United States Earthquakes* for the post-1930 events, in Townley-Allen (1939) for the 1901 and 1922 Parkfield events as interpreted by USGS/NEIC, and in Top-

Table 5
Confidence Parameters

(a) Location of Epicentral Region

No. of MMI	rms [M_I] Contour				
	95%	90%	80%	67%	50%
5	0.589	0.469	0.352	0.259	0.179
7	0.482	0.392	0.287	0.208	0.138
10	0.387	0.303	0.217	0.152	0.098
15	0.287	0.221	0.152	0.102	0.062
20	0.226	0.169	0.113	0.074	0.044
25	0.188	0.138	0.093	0.059	0.035
30	0.156	0.118	0.078	0.050	0.030
40	0.124	0.093	0.062	0.040	0.024
50	0.106	0.079	0.053	0.034	0.021
60	0.095	0.072	0.048	0.031	0.019
70	0.087	0.066	0.045	0.028	0.017
80	0.080	0.061	0.041	0.026	0.016
90	0.076	0.059	0.039	0.025	0.015
100	0.072	0.056	0.038	0.024	0.014
110	0.070	0.054	0.036	0.023	0.014
120	0.068	0.052	0.035	0.022	0.013
130	0.066	0.051	0.034	0.021	0.013
150	0.063	0.049	0.032	0.020	0.013
170	0.060	0.047	0.031	0.019	0.012

(b) M

No. of MMI	Limits				
	95%	90%	80%	67%	50%
5	−0.72, 0.53	−0.56, 0.46	−0.42, 0.38	−0.29, 0.31	−0.18, 0.24
7	−0.62, 0.47	−0.50, 0.41	−0.36, 0.35	−0.26, 0.28	−0.17, 0.21
10	−0.54, 0.42	−0.44, 0.37	−0.33, 0.31	−0.24, 0.25	−0.15, 0.19
15	−0.48, 0.37	−0.39, 0.33	−0.30, 0.28	−0.22, 0.23	−0.14, 0.18
20	−0.45, 0.35	−0.36, 0.31	−0.28, 0.26	−0.21, 0.22	−0.14, 0.17
25	−0.42, 0.33	−0.35, 0.29	−0.27, 0.25	−0.21, 0.21	−0.14, 0.17
30	−0.40, 0.32	−0.34, 0.28	−0.27, 0.24	−0.20, 0.20	−0.14, 0.16
40	−0.38, 0.30	−0.33, 0.27	−0.26, 0.23	−0.20, 0.20	−0.14, 0.16
50	−0.37, 0.29	−0.31, 0.26	−0.26, 0.22	−0.20, 0.19	−0.13, 015
60	−0.36, 0.28	−0.31, 0.25	−0.25, 0.22	−0.20, 0.19	−0.14, 0.15
70	−0.35, 0.28	−0.30, 0.25	−0.25, 0.22	−0.20, 0.19	−0.14, 0.15
80	−0.34, 0.27	−0.30, 0.24	−0.25, 0.22	−0.20, 0.18	−0.14, 0.15
90	−0.33, 0.26	−0.29, 0.24	−0.25, 0.22	−0.20, 0.18	−0.14, 0.15
100	−0.33, 0.26	−0.29, 0.24	−0.25, 0.21	−0.20, 0.18	−0.14, 0.15
110	−0.33, 0.26	−0.29, 0.24	−0.25, 0.21	−0.20, 0.18	−0.14, 0.15
120	−0.32, 0.26	−0.29, 0.24	−0.25, 0.21	−0.20, 0.18	−0.14, 0.15
130	−0.32, 0.25	−0.29, 0.24	−0.25, 0.21	−0.20, 0.18	−0.14, 0.15
150	−0.31, 0.25	−0.28, 0.23	−0.25, 0.21	−0.20, 0.18	−0.14, 0.14
170	−0.31, 0.25	−0.28, 0.23	−0.24, 0.21	−0.20 0.18	−0.15, 0.14

Figure 10. 95% confidence limits of **M**: (a) for 30 MMI shown as dots, open squares, and open diamonds for strike slip (including Loma Prieta), thrust, and normal faulting training-set events, respectively; (b) for different quantities of MMI data.

pozada *et al.* (1981) for the 1881 Parkfield event were culled using the procedures described above for the training-set events. The vetted intensity data for the test-set events are summarized in Table 2. M_I and rms [M_I] were calculated for the test-set events using the procedures described above for the training-set events. In particular, we test the three-step analysis strategy proposed above.

Kettleman Hills Earthquake

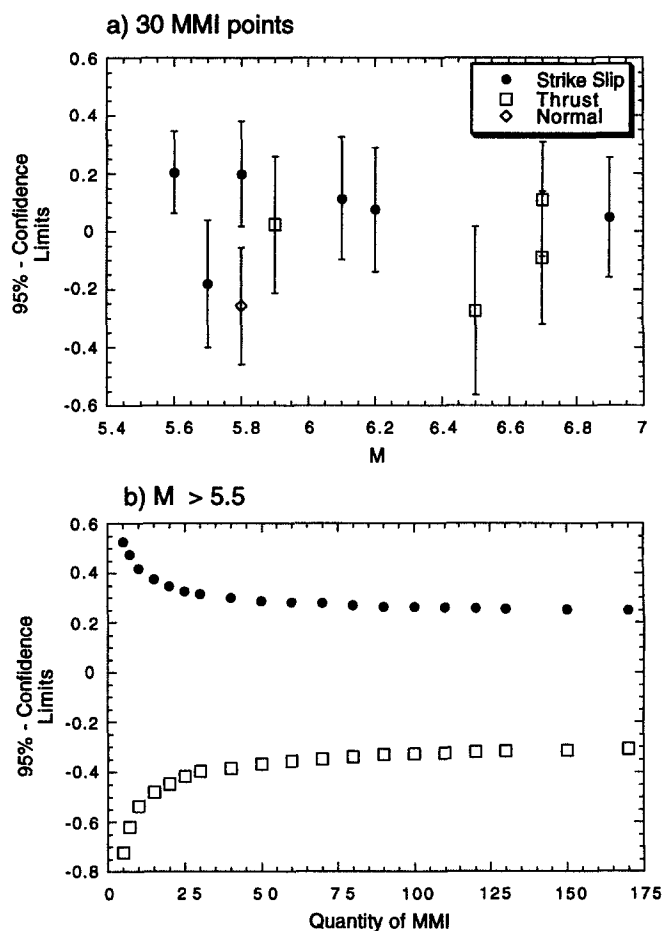The 4 August 1985 **M** = 6.1 Kettleman Hills earthquake occurred on a blind-thrust fault beneath the Kettleman Hills North Dome anticline 15 km southeast of the 1983 Coalinga mainshock. The instrumental epicenter lies on the 90% confidence contour (Fig. 11a). Since the inferred rupture extended about 20 km southeast of the mainshock instrumental epicenter (Ekström *et al.*, 1992), the rupture zone extends within the 50% confidence-level contour. At the instrumental epicenter, M_I = 5.8, midway between **M** = 6.1 and M_L = 5.6. The rate of moment release in the Kettleman Hills earthquake was unusually slow with a depletion of radiated high-frequency seismic energy (Ekström *et al.*, 1992), so finding M_I less than **M** is not surprising.

Santa Rosa Earthquakes

Two earthquakes with M_L = 5.6 and 5.7 occurred near Santa Rosa on 2 October 1969 near the northwest end of the Rodgers Creek fault (Wong and Bott, 1995). Because these earthquakes occurred only 82 min apart, their intensity data are merged in *United States Earthquakes* (von Hake and Cloud, 1971). The instrumental epicenters lie within the 90% confidence-level contour, but outside the 50%, 67%, and 80% confidence-level epicentral boundaries (Fig. 11b). The
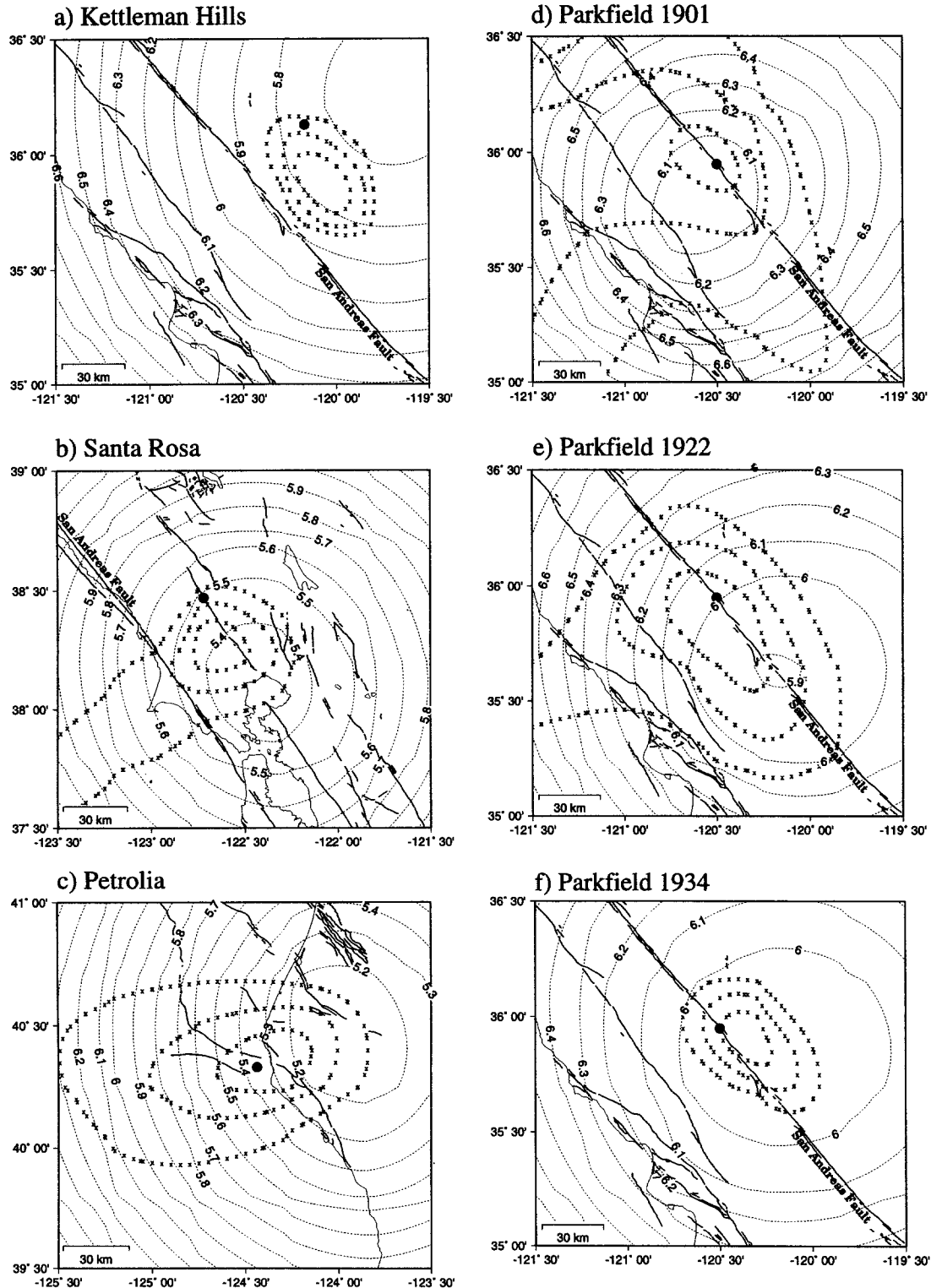
Figure 11. Maps of contours of $\mathbf{M}_I$ as thin dashed lines and instrumental epicenters as dots for (a) Kettleman Hills, (b) Santa Rosa, (c) Petrolia, (d) Parkfield 1901, (e) Parkfield 1922, and (f) Parkfield 1934 earthquakes. The epicenter of the Parkfield 1966 event is the epicenter plotted in (d), (e), and (f). The rms [$\mathbf{M}_I$] contours corresponding to the 50%, 80%, and 95% confidence levels for location are shown as the innermost, middle, and outermost contours of Xs, respectively. We used the contour values listed in Table 5 for 170 MMI in (a) and (b), 40 MMI in (c), 10 MMI in (d), 15 MMI in (e), and 100 MMI in (f). California coastline and <700 ka Quaternary faults (Jennings, 1992) are shown as thin and thick lines, respectively.

contours extend west beyond the San Andreas fault; that is, the confidence-level contours are elongated in the direction of sparse MMI data. It would be difficult to exclude with a high degree of confidence a San Andreas fault source for the Santa Rosa earthquakes if only intensity data were available. For a location on the Rodgers Creek fault (the most likely source within the 50% confidence-level contour), $M_I = 5.4$. At the instrumental epicenters, $M_I = 5.6$.

Petrolia Earthquake

The $M = 5.2$ Petrolia event on 21 November 1986 is a strike-slip earthquake located on the Mendocino Fracture Zone near the Cape Mendocino coast. Intensity data are only available for easterly azimuths (N17°E to S26°E), and site corrections are available for only 7 of the 41 reporting sites, and these are poorly determined (six are based on one hit and one on two hits). Poorly determined site corrections, such as those available for the Cape Mendocino area from the distant training-set earthquakes, likely do not improve M_I estimates of M and thus will not be used. The instrumental epicenter lies within all the confidence-level contours (see Fig. 11c). M_I at the instrumental epicenter is 5.4.

Parkfield Earthquakes

Four of the test-set events are Parkfield earthquakes that occurred in 1881, 1901, 1922, and 1934. The consistency of instrumental observations and accounts for the 1922, 1934, and 1966 events, together with similar descriptions of the 1881 and 1901 events, led Bakun and McEvilly (1984) to hypothesize that these are all "characteristic Parkfield earthquakes" with common location and seismic moment. Abe (1988) subsequently determined $M_S = 6.4 \pm 0.2$ for the 1901 event, consistent with the Parkfield characteristic earthquake hypothesis.

The rupture zone of the 1966 Parkfield earthquake extends from the 1966 epicenter, plotted as a dot in Figures 11d through 11f, southeast about 20 km (Lindh and Boore, 1981). Note that the instrumental epicenter for the 1922 earthquake lies at or a few kilometers northwest of the 1966 epicenter (Bakun and McEvilly, 1984) and that this shock broke petroleum pipelines that cross the San Andreas fault about 30 km southeast of the 1966 epicenter (G. B. Moody, Chevron U.S.A. internal report, 1934), so that the 1922 event likely ruptured the entire 1966 rupture length.

M_I at the 1966 instrumental epicenter is 6.0 for Parkfield 1901, 6.0 for Parkfield 1922, and 5.9 for Parkfield 1934, so that M estimated from intensity data is the same for these events. Part of the 1966 rupture zone lies within all of confidence-level contours for the 1901, 1922, 1934, and 1966 Parkfield earthquakes so that the epicentral regions estimated from intensity data are the same for these events. That is, the location and M for the 1901, 1922, 1934, and 1966 Parkfield earthquakes estimated from intensity data overlap and are in agreement with the instrumental locations and M, consistent with the characteristic Parkfield earthquake hypothesis.

The seven damage reports for the 1881 earthquake were found by Toppozada et al. (1981) by chance while researching other earthquakes (Toppozada, 1985). While the descriptions were sufficient to assign an intensity value to Imusdale, the ancestral settlement at the town of Parkfield, the other descriptions—"heavy" at Hollister, "felt" at Santa Cruz, Salinas, San Luis Obispo, and Visalia, and "light" at Lemoore—are not sufficient to assign unambiguous intensity values. Written accounts of the 1881 earthquake clearly identify surface breaks on the southwest fracture zone of the Parkfield section of the San Andreas fault (Toppozada, written comm., 1985), so that in this case (fortunately), the location does not depend solely on intensity data. If we use the instrumental epicenter of the 1966 earthquake and assume that "heavy" implies MMI V or VI (use V 1/2) and "light" or "felt" implies MMI III or IV (use III 1/2), $M_I = 5.8$. This is consistent with the characteristic Parkfield earthquake hypothesis. Using MMI III for the felt and light observations and MMI V for the heavy report as the low-end estimate, M_I is 5.2. Using MMI IV for the felt and light observations and MMI VI for the heavy report as the high-end estimate, M_I is 6.0. While the high-end estimate is consistent with the characteristic Parkfield earthquake hypothesis, the low-end estimate is not. These very different end-member estimates suggest that the intensity data for the 1881 event are near the margin of data sufficient for analysis. These difficulties are minor, however, compared with those in constructing isoseismals from the same data (see Toppozada et al., 1981).

Basin and Range Earthquakes in Eastern California

The $M = 6.4$ 1986 Chalfant earthquake and the $M = 5.9$ 1966 Truckee earthquake occurred just east of the Sierra Nevada in the Basin and Range tectonic province (see Fig. 1), whereas all the training-set earthquakes occurred in western California. Evernden's (1975) regional attenuation factor k separates coastal ($k = 1\frac{3}{4}$) and eastern ($k = 1\frac{1}{2}$) California so that applicability of M_I in eastern California must be demonstrated; in fact, the analysis procedures fail for these Basin and Range events. First, the instrumental epicenters each lie outside the 95% confidence-level contours and about 50 km northeast of the center of the region bounded by the 50% confidence-level contour. Second, M_I for Chalfant at its instrumental epicenter is 6.7 and M_I for the Truckee earthquake at its instrumental epicenter is 6.5. One explanation for these discrepancies is lower attenuation for Basin and Range paths and/or for paths traversing the crystalline rocks of the Sierra Nevada. Additional Basin and Range test earthquakes are necessary to clarify if and how the intensity analysis procedures presented here might be modified for use in eastern California and Nevada.

Discussion

An improved method for estimating M from intensity observations, similar to that used by Evernden et al. (1981), has been presented that uses the intensity observations di-

rectly, rather than the areas enclosed by isoseismal lines. There are significant advantages in using individual intensity observations directly. First, the procedures are explicit so that the results are reproducible. Second, uncertainties corresponding to any desired level of confidence can be calculated. Use of several confidence levels should be useful in considering multiple alternative source parameter hypotheses in a decision tree. Finally, site corrections can be applied.

The results obtained with a set of independent test-set earthquakes are consistent with the confidence-level parameters established for the training-set earthquakes. That is, epicenters for all six western California test-set earthquakes lie within the 95% confidence-level contours; epicenters or rupture zones for all six lie within the 90% confidence-level contour; epicenters or rupture zones for five of the six lie within the 80%, 67%, and 50% confidence-level contours; and epicenters for three of the six lie within the 50% confidence-level contours given in Table 5a. The confidence limits for M can be tested using the four western California test-set events for which independent estimates of M are available: $M - M_I = 0.35, -0.15, 0.1,$ and 0.2 for Kettleman Hills, Petrolia, Parkfield 1922, and Parkfield 1934, respectively. $M - M_I$ for two of the four are within the corresponding 50% confidence-level limits of M, and $M - M_I$ for three of the four are within the corresponding 95%, 90%, 80%, and 67% confidence-level limits of M. These results are not inconsistent with the confidence-level limits for M given in Table 5b.

Site Corrections

Thus far, we have justified site corrections as a means of accounting for differences in site conditions and through marginal improvements for the $M > 5.5$ training-set earthquakes in the estimates of M from M_I and by better coincidence of the location of rupture zone and the region of minimum rms [M_I]. Given the additional complications that they introduce, are site corrections significant in the analysis? Well-determined site corrections were not available for the Petrolia test-set earthquake, yet satisfactory results were obtained there without applying site corrections (see Fig. 11c). While not necessary, site corrections do improve the results significantly for the other test-set earthquakes. Compare the contours of M_I and rms [M_I] in Figure 11 with those obtained without site corrections in Figure 12. The differences in M_I near the epicentral regions are all small, 0.1 or less. However, the areas bounded by the confidence-level contours are significantly larger without site corrections for the three earlier Parkfield test-set events with fewer MMI observations; the size of the areas bounded by the contours for the Kettleman Hills and Santa Rosa events with many MMI observations are of comparable size. That is, site corrections provide significantly tighter bounds on the epicentral area for earlier events with fewer MMI. Also, with site corrections, there is significantly better correlation of the instrumental epicenters and rupture areas with the bounded epicentral regions, even though they are of comparable size

or smaller. While the results without site corrections are good, they are significantly better with site corrections.

Stress Drop

If the larger $M - M_I$ for the Kettleman Hills event is due to a slow rate of moment release, how much of the $M - M_I$ differences might be ascribed to other source parameters? Stress drop, the stress regime, and the depth range of energy radiation are source parameters that affect the characteristics of the seismic energy, and thus potentially $M - M_I$.

Atkinson and Hanks (1995) define a high-frequency magnitude scale m, suggest that the difference between M and m provides a measure of stress drop, and tabulate m for 10 of this study's training-set events. The rms $(m - M_I)$ for these training-set events is 0.24; the comparable rms $(M - M_I)$ and rms $(M_L - M_I)$ are 0.20 and 0.21, respectively. That is, the match of M_I to M and to M_L are comparable and both are better than the match of M_I to m. That is, adjustment of the M_I, using either m or M_L, to account for stress drop apparently would not improve the overall fit of M_I to M. While stress drop may not be an important parameter in explaining these California earthquake intensities, the variability in stress drop for earthquakes in the eastern United States is much larger than for earthquakes in California (Atkinson and Hanks, 1995); the strong dependence of high-frequency ground motion on stress drop (Hanks and Johnston, 1992) suggests that stress drop may be an important consideration in applying these techniques to the eastern United States and, perhaps, other regions.

Style of Faulting and Focal Depth

For a given M, peak ground accelerations increase with the depth of the seismic source, and the rate of increase for strike-slip faulting earthquakes lies between the greater rate for thrust-faulting earthquakes and the lesser rate for normal-faulting earthquakes (McGarr, 1984). If intensity varies with peak acceleration, then $M - M_I$ should decrease with the depth of the moment centroid, and $M - M_I$ for strike-slip sources should be intermediate between smaller and larger $M - M_I$ for thrust- and normal-faulting sources, respectively. The mean [$M - M_I$] = 0.01 ± 0.05 for the seven "pure" strike-slip sources is greater than the mean [$M - M_I$] = -0.10 ± 0.09 for the nine thrust sources shown in Figure 13, consistent with McGarr's peak acceleration data and the assumption that intensity varies with peak acceleration; no conclusions can be drawn from the single $M - M_I = -0.2$ value obtained for the normal-faulting Oroville earthquake. There is no apparent overall depth dependence in the $M - M_I$ shown in Figure 13, perhaps because the moment centroids for nearly all of these events likely are at comparable crustal depths. Note, however, that for the seven Coalinga events, two of which are relatively small shocks ($M = 5.4$ and 5.1) at shallower ($h = 2.4$ km) and deeper ($h = 12$ km) depths, respectively, $M - M_I$ decreases nearly linearly with depth, consistent with McGarr's peak acceler-
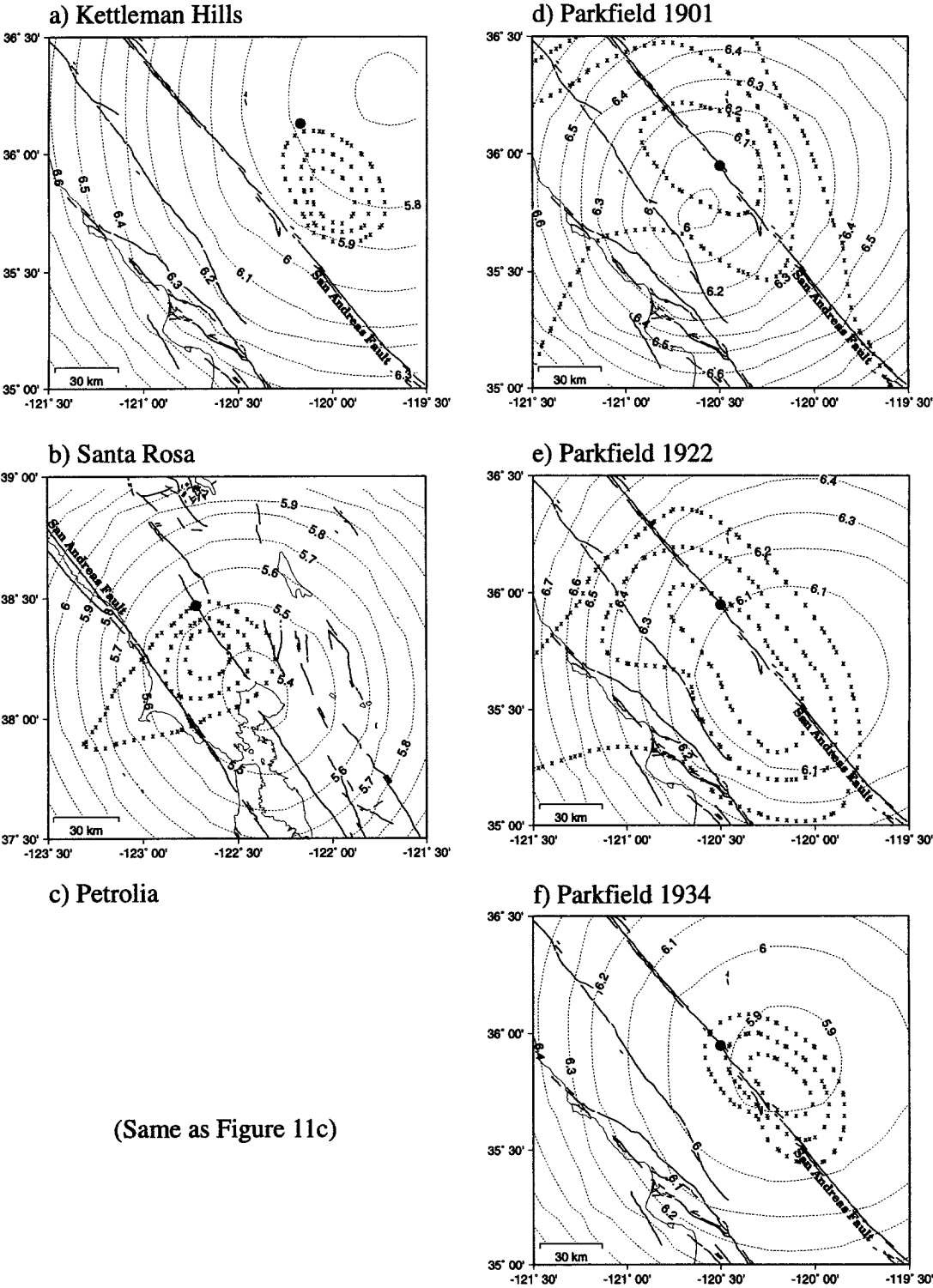
a) Kettleman Hills

b) Santa Rosa

c) Petrolia

(Same as Figure 11c)

d) Parkfield 1901

e) Parkfield 1922

f) Parkfield 1934

Figure 12.   Maps of contours of M_I and rms $[M_I]$ without applying site corrections.
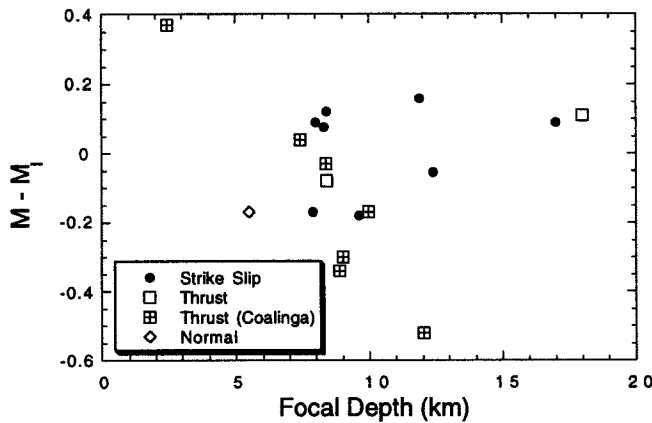See caption of Figure 11.

Figure 13. $\mathbf{M} - \mathbf{M}_I$ versus focal depth for the 18 training-set events with independent determinations of $\mathbf{M}$.

ation data and the assumption that intensity scales with peak acceleration.

Caveats

Applying the empirical confidence levels in Table 5, obtained from the recent training-set earthquakes, to earlier events with sparse data implicitly assumes that the random samples of the training-set MMI data are not dissimilar from the sparse MMI data of the earlier events and that source and other parameters not explicitly used in the formulation have little impact on the statistical relation of $\mathbf{M}$ and $\mathbf{M}_I$ and of epicenter location and rms $[\mathbf{M}_I]$. For example, the distributions of intensity observations versus epicenter-to-observation point distance and azimuth should not be dissimilar. The distributions of MMI will be similar if drawn from the same population of source regions and observation sites. This is almost the case for earlier events located in northern California west of the Sierra Nevada: Early settlements in this region were located in the same places where population centers are located today, and newspaper accounts of the effects of early earthquakes can be gauged using the MMI scale.

The training set includes strike-slip, thrust, oblique-slip, and normal-faulting sources; sources spanning the range of California seismogenic focal depths; and sources with unilateral and bilateral rupture expansion. While these parameters do not significantly bias $\mathbf{M}_I$ or the relation of rms $[\mathbf{M}_I]$ to epicentral region location for the $\mathbf{M} > 5.5$ training-set events, the style of faulting, stress drop, and the depth of the earthquake source can all affect $\mathbf{M}_I$. For the training-set events, $\mathbf{M} - \mathbf{M}_I$ is -0.1 on average for the thrust-faulting sources. Stress drop and the depth of the moment centroid generally do not vary significantly for California earthquakes, although $\mathbf{M}_I$ for particularly shallow and/or particularly low stress-drop sources are likely to be underestimates of $\mathbf{M}$. Conversely, $\mathbf{M}_I$ for particularly deep and/or particularly high stress-drop sources are likely to overestimate $\mathbf{M}$. Although such shocks are uncommon, the 21 February 1973

$\mathbf{M} = 5.3$ Point Mugu earthquake that occurred at a depth of 17 km beneath the southern front of the Transverse Ranges in southern California was an unusually deep and an unusually high stress-drop source (Ellsworth et al., 1973). $\mathbf{M}_I$ at the instrumental epicenter for the Pt. Mugu earthquake is 6.2 ± 0.3, more consistent with the $\mathbf{M}_L = 5.9$ for this shock than with $\mathbf{M} = 5.3$ (Bakun and Dewey, 1997).

While we have found an empirical robust and reliable estimator of source parameters for earthquakes in northern California west of the Sierra Nevada, we have not provided a fundamental rationalization of intensity. As already noted, any relation of a qualitatively defined intensity scale and quantitative seismology is fortuitous. Our empirically derived analysis strategy yields reliable source parameter estimates for a particular population of earthquake sources— in a particular region, a particular range of earthquake size, etc. Our empirical results may be useful in estimating source parameters in other regions, for very large earthquakes, etc., but the procedures must be evaluated, calibrated, and perhaps modified before being used in other applications.

Conclusions

Modified Mercalli intensities (MMI) for 22 post-1965 central and southern California earthquakes $(4.4 < \mathbf{M} < 6.9)$ were used to construct an analysis strategy to bound the epicentral region and the moment magnitude $\mathbf{M}$ using individual intensity observations. $\mathbf{M}$ from intensity observations is $\mathbf{M}_I = \text{mean} (\mathbf{M}_i)$, where $\mathbf{M}_i = (\text{MMI}_i + 3.29 + 0.0206 * \Delta_i)/1.68$, and Δ_i is the epicentral distance (km) of observation MMI$_i$. The epicentral region is bounded by contours of rms $[\mathbf{M}_I] = [\text{rms} (\mathbf{M}_I - \mathbf{M}_i) - \text{rms}_0 (\mathbf{M}_I - \mathbf{M}_i)]$, where rms$_0 (\mathbf{M}_I - \mathbf{M}_i)$ is the minimum rms over a grid of assumed epicenters, and a distance weighting function

$$W_i = \begin{cases} 0.1 + \cos [(\Delta_i/150) * \pi/2], & \text{for } \Delta_i < 150 \text{ km,} \\ 0.1, & \text{for } \Delta_i > 150 \text{ km,} \end{cases}$$

and empirical site corrections are used.

We propose a three-step strategy:

1. Calculate $\mathbf{M}_I$ and rms $[\mathbf{M}_I]$ over a grid of trial epicenters.
2. The rms $[\mathbf{M}_I]$ contours bound the epicentral region with levels of confidence appropriate for the quantity of MMI observations. The contour values for 95%, 90%, 80%, 67%, and 50% confidence levels are listed in Table 5a.
3. $\mathbf{M}_I$ at tectonically attractive epicenters within the appropriate confidence-level contours are the best estimates of $\mathbf{M}$ for those assumed epicenters. The uncertainty in $\mathbf{M}$ appropriate for different confidence levels and quantities of MMI observations are listed in Table 5b.

The epicentral region bounds and the bounds on $\mathbf{M}$ obtained applying this strategy to an independent test set of western California earthquakes are consistent with the instrumental epicenters and $\mathbf{M}$. We did not obtain satisfactory results for

the 1966 Truckee and 1986 Chalfant earthquakes that occurred in eastern California within the Basin and Range tectonic province, which reinforces our caveat that the analysis strategy must be tested before being used to analyze earthquake intensity data in other areas.

The analysis strategy is particularly appropriate for the analysis of earthquakes for which the only available data are a sparse set of intensity observations.

Acknowledgments

References

Abe, K. (1988). Magnitudes and origin times from Milne seismograph data: earthquakes in China and California, 1898–1912, in *Historical Seismograms and Earthquakes of the World: San Diego, Calif.*, W. H. K. Lee, H. Meyers, and K. Shimizaki (Editors), Academic Press, New York, pp. 37–50.

Atkinson, G. M. and T. C. Hanks (1995). A high-frequency magnitude scale, *Bull. Seism. Soc. Am.* **85,** 825–833.

Bakun, W. H. and T. V. McEvilly (1984). Recurrence models and Parkfield, California, earthquakes, *J. Geophys. Res.* **89,** 3051–3058.

Bakun, W. H. and J. W. Dewey (1997). Earthquake location and magnitude of southern California earthquakes from seismic intensity data (abstract), *Seism. Res. Lett.* **68,** 321.

Bennett, J. H. and R. W. Sherburne (1983). The 1983 Coalinga, California earthquakes, *Calif. Div. Mines Geol. Spec. Publ. 66,* 335 pp.

Bolt, B. A., T. V. McEvilly, and R. A. Uhrhammer (1981). The Livermore Valley, California, sequence of January 1980, *Bull. Seism. Soc. Am.* **71,** 451–463.

Borcherdt, R. D. and G. Glassmoyer (1994). Influences of local geology on strong and weak ground motions recorded in the San Francisco Bay region and their implications for site-specific building-code provisions, in *The Loma Prieta, California, Earthquake of October 17, 1989—Strong Ground Motion*, R. D. Borcherdt, (Editor), *U.S. Geol. Surv. Profess. Pap. 1551-A,* A77–A108.

Borcherdt, R. D. (1994). Estimates of site-dependent response spectra for design (methodology and justification), *Earthquake Spectra* **10,** 617–653.

Borcherdt, R. D., C. M. Wentworth, G. Glassmoyer, T. Fumal, P. Mork, and J. Gibbs (1991). On the observation and predictive GIS mapping of ground response in the San Francisco Bay region, California, *Fourth International Conference on Seismic Zonation, Stanford, California, Proceedings*, Vol. III, 545–552.

Coffman, J. L. and C. W. Stover (1984). United States Earthquakes, 1975, *U.S. Geol. Surv. Open-File Rept. 84-975,* 136 pp.

Coffman, J. L. and C. A. von Hake (1984). United States Earthquakes, 1971, *U.S. Geol. Surv. Open-File Rept. 84-971,* 175 pp.

Dewey, J. W., B. G. Reagor, L. Dengler, and K. Moley (1995). Intensity distribution and isoseismal maps for the Northridge, California earthquake of January 17, 1994, *U.S. Geol. Surv. Open-File Rept. 95-92,* 35 pp.

Ekström, G., R. S. Stein, J. P. Eaton, and D. Eberhart-Phillips (1992). Seismicity and geometry of a 110-km-long blind thrust fault 1. The 1985

Kettleman Hills, California, earthquake, *J. Geophys. Res.* **97,** 4843–4864.

Ellsworth, W. L., R. H. Campbell, D. P. Hill, R. A. Page, R. W. Alewine III, T. C. Hanks, T. H. Heaton, J. A. Hileman, H. Kanamori, B. Minster, and J. H. Whitcomb (1973). Point Mugu, California, earthquake of 21 February 1973 and its aftershocks, *Science* **182,** 1127–1129.

Ellsworth, W. L. (1990). Earthquake history, 1769–1989, *The San Andreas Fault System, California*, R. E. Wallace (Editor), Chap. 6, *U.S. Geol. Surv. Profess. Pap. 1515,* 153–188.

Evernden, J. F. (1975). Seismic intensities, "size" of earthquakes and related parameters, *Bull. Seism. Soc. Am.* **65,** 1287–1313.

Evernden, J. F., W. M. Kohler, and G. D. Clow (1981). Seismic intensities of earthquakes in the conterminous United States—their prediction and interpretation, *U.S. Geol. Surv. Profess. Pap. 1223,* 56 pp.

Hanks, T. C., J. A. Hileman, and W. Thatcher (1975). Seismic moments of the larger earthquakes of the southern California region, *Geol. Soc. Am. Bull.* **86,** 1131–1139.

Hanks, T. C. and H. Kanamori (1979). A moment magnitude scale, *J. Geophys. Res.* **84,** 2348–2350.

Hanks, T. C. and A. C. Johnston (1992). Common features of the excitation and propagation of strong ground motion for North American earthquakes, *Bull. Seism. Soc. Am.* **82,** 1–23.

Helley, E. J. and K. R. Lajoie (1979). Flatland deposits of the San Francisco Bay Region, California—their geology and engineering properties, and their importance to comprehensive planning, *U.S. Geol. Surv. Profess. Pap. 943,* plate 3, map scale 1:125,000.

Howell, B. F. and T. R. Schulz (1975). Attenuation of Modified Mercalli intensity with distance from the epicenter, *Bull. Seism. Soc. Am.* **65,** 651–665.

Jennings, C. W. (1977). Geologic map of California: California Division of Mines and Geology, Geologic Data Map No. 2, map scale 1:750,000.

Jennings, C. W. (1992). Preliminary fault activity map of California, *Calif. Div. Mines Geol. Open-File Rep. 92-03,* map scale 1:750,000.

Lindh, A. G. and D. M. Boore (1981). Control of rupture by fault geometry during the 1966 Parkfield earthquake, *Bull. Seism. Soc. Am.* **71,** 95–116.

McGarr, A. (1984). Scaling of ground motion parameters, state of stress, and focal depth, *J. Geophys. Res.* **89,** 6969–6979.

Neumann, F. (1936). United States Earthquakes 1934, *U.S. Coast Geodetic Surv.*, Washington, D.C., 101 pp.

Real, C. R. (1985). Ground rupture during the 1901 Parkfield earthquake (abstract), *EOS* **66,** 982.

Rymer, M. J. and W. L. Ellsworth (1990). The Coalinga, California earthquake of May 2, 1983, *U.S. Geol. Surv. Profess. Pap. 1487,* 417 pp.

Somerville, P. and J. Yoshimura (1990). The influence of critical Moho reflections on strong ground motions recorded in San Francisco and Oakland during the 1989 Loma Prieta earthquake, *Geophys. Res. Lett.* **17,** 1203–1206.

Stover, C. W. and C. A. von Hake (1982). United States Earthquakes, 1980, *U.S. Geol. Surv. NOAA,* Golden, Colorado, 170 pp.

Stover, C. W. and C. A. von Hake (1984). United States Earthquakes, 1979, *U.S. Geol. Surv. Open-File Rept. 84-979,* 170 pp.

Stover, C. W. (1984). United States Earthquakes, 1981, *U.S. Geol. Surv. Open-File Rept. 84-981,* 136 pp.

Stover, C. W. (1987). United States Earthquakes, 1983, *U.S. Geol. Surv. Bull. 1698,* 196 pp.

Stover, C. W. (1988). United States Earthquakes, 1984, *U.S. Geol. Surv. Bull. 1862,* 179 pp.

Stover, C. W. and L. R. Brewer (1991). United States Earthquakes, 1985, *U.S. Geol. Surv. Bull. 1954,* 170 pp.

Stover, C. W. and L. R. Brewer (1994). United States Earthquakes, 1986, *U.S. Geol. Surv. Bull. 2089,* 240 pp.

Stover, C. W., B. G. Reagor, F. W. Baldwin, and L. R. Brewer (1990). Preliminary isoseismal map for the Santa Cruz (Loma Prieta), California, earthquake of October 18, 1989 UTC, *U.S. Geol. Surv. Open-File Rept. 90-18,* 24 pp.

Toppozada, T. R. (1975). Earthquake magnitude as a function of intensity data in California and western Nevada, *Bull. Seism. Soc. Am.* **65,** 1223–1238.

Toppozada, T. R., C. R. Real, and D. L. Parke (1981). Preparation of iso-seismal maps and summaries of reported effects for Pre-1900 California earthquakes, *Calif. Div. Mines Geol. Open-File Rept. 81-11 SAC,* 182 pp.

Toppozada, T. R. (1985). Questioning the regular recurrence of characteristic Parkfield earthquakes (abstract), *EOS* **66,** 982.

Townley, S. D. and M. W. Allen (1939). Descriptive catalog of earthquakes of the Pacific Coast of the United States 1769 to 1928, *Bull. Seism. Soc. Am.* **29,** 297 pp.

Uhrhammer, R. A. (1981). The Pacifica earthquake of 28 April 1979, *Bull. Seism. Soc. Am.* **71,** 1161–1172.

U.S. Geological Survey (1995). GNIS Geographical Names Information System Digital Gazetteer (CD ROM).

von Hake, C. A. and W. K. Cloud (1968). United States Earthquakes, 1966, *U.S. Coast Geodetic Surv.,* Washington, D.C., 110 pp.

von Hake, C. A. and W. K. Cloud (1971). United States Earthquakes, 1969, *U.S. Coast Geodetic Surv.,* Washington, D.C., 80 pp.

Wald, D. J., T. H. Heaton, and K. W. Hudnut (1996). The slip history of the 1994 Northridge, California, earthquake determined from strong-motion, teleseismic, GPS, and leveling data, *Bull. Seism. Soc. Am.* **86,** S49–S70.

Wentworth, C. M. (1993). General distribution of geologic materials in the southern San Francisco Bay region, California: a digital map database, *U.S. Geol. Surv. Open-File Rept. 93-693,* map scale 1:125,000.

Wessel, P. and W. H. F. Smith (1991). Free software helps map and display data, *EOS* **72,** 441, 445–446.

Wood, H. O. and F. Neumann (1931). Modified Mercalli intensity scale of 1931, *Bull. Seism. Soc. Am.* **21,** 277–283.

Wong, I. G. and J. D. J. Bott (1995). A new look at the 1969 Santa Rosa, California, earthquakes, *Bull. Seism. Soc. Am.* **85,** 334–341.

U.S. Geological Survey
345 Middlefield Rd. MS977
Menlo Park, California 94025